Matrix Biology Plus 24 (2024) 100160

Contents lists available at ScienceDirect

Matrix Biology Plus

journal homepage: www.sciencedirect.com/journal/matrix-biology-plus

The importance of matrix in cardiomyogenesis: Defined substrates for maturation and chamber specificity

Jake Ireland [a], Kristopher A. Kilian [a,b,c,*]

[a] School of Chemistry, UNSW Sydney, Sydney, New South Wales, Australia
[b] School of Materials Science and Engineering, UNSW Sydney, Sydney, New South Wales, Australia
[c] Australian Centre for NanoMedicine, UNSW Sydney, Sydney, New South Wales, Australia

ARTICLE INFO

Keywords:
Extracellular Matrix Proteins
Cardiomyocyte Differentiation
Chamber Specification
Action Potential Morphology
Array Platform
Cardiomyocyte Maturation

ABSTRACT

Human embryonic stem cell-derived cardiomyocytes (hESC-CM) are a promising source of cardiac cells for disease modelling and regenerative medicine. However, current protocols invariably lead to mixed population of cardiac cell types and often generate cells that resemble embryonic phenotypes. Here we developed a combinatorial approach to assess the importance of extracellular matrix proteins (ECMP) in directing the differentiation of cardiomyocytes from human embryonic stem cells (hESC). We did this by focusing on combinations of ECMP commonly found in the developing heart with a broad goal of identifying combinations that promote maturation and influence chamber specific differentiation. We formulated 63 unique ECMP combinations fabricated from collagen 1, collagen 3, collagen 4, fibronectin, laminin, and vitronectin, presented alone and in combinations, leading to the identification of specific ECMP combinations that promote hESC proliferation, pluripotency, and germ layer specification. When hESC were subjected to a differentiation protocol on the ECMP combinations, it revealed precise protein combinations that enhance differentiation as determined by the expression of cardiac progenitor markers kinase insert domain receptor (KDR) and mesoderm posterior transcription factor 1 (MESP1). High expression of cardiac troponin (cTnT) and the relative expression of myosin light chain isoforms (MLC2a and MLC2v) led to the identification of three surfaces that promote a mature cardiomyocyte phenotype. Action potential morphology was used to assess chamber specificity, which led to the identification of matrices that promote chamber-specific cardiomyocytes. This study provides a matrix-based approach to improve control over cardiomyocyte phenotypes during differentiation, with the scope for translation to cardiac laboratory models and for the generation of functional chamber specific cardiomyocytes for regenerative therapies.

Introduction

It has been two decades since cardiac cell therapies were first investigated with the initial hypothesis that non-contracting stem cells could transdifferentiate when injected into an infarct region [1,2]. Despite the promising benefits of pre-clinical trials, cell therapies in larger animals appeared to interfere with native electrical conduction [3]. The decades since have seen tremendous improvements in cardiac modelling and regenerative medicines as the field of pluripotent stem cell research has expanded. The use of human embryonic stem cells (hESC) and human induced pluripotent stem cells (hiPSC) has provided alternative options to primary cells for investigating cardiomyogenisis [4], exploring cardiomyocyte lineage specification [5], and has pioneered the field of engineered heart muscle (EHM) as alternative delivery methods of stem cells to infarct regions [6,7]. Contracting cardiomyocytes developed from human embryonic stem cells, known as human embryonic stem cell-derived cardiomyocytes (hESC-CM), have been cultured in laboratories around the world with some incredible advances in mimicking the morphologic and phenotypic qualities of the adult heart [8,9]. The efficiency of differentiating cardiomyocytes from a pluripotent cell source is nearing 100 % for most modern protocols [10] but issues persist that prohibit these cells from entering clinical use [11,12]. Currently clinical translation for stem cell derived cardiomyocytes face controversy regardless of the cell source as hESC pose ethical dilemmas and hiPSC struggle to find a footing in clinical translation due to genetic changes required for pluripotent cell generation

* Corresponding author at: School of Chemistry, UNSW Sydney, Sydney, New South Wales, Australia.
E-mail address: k.kilian@unsw.edu.au (K.A. Kilian).

https://doi.org/10.1016/j.mbplus.2024.100160
Received 7 February 2024; Received in revised form 15 August 2024; Accepted 16 August 2024
Available online 20 August 2024

[103,104]. In this study we chose to work with hESC because they have extant success in clinical translation to treat ischemic cardiac conditions in humans and serves as a reliable cell source for modelling cardiac differentiation in vitro [105]. The criteria for a protocol to meet clinical standards require phenotypic and electrophysiological purity, a high differentiation efficiency, and an absence of adverse effects in pre-clinical animal models [13]. Whilst differentiation efficiency can be achieved, most protocols give rise to a heterogeneous population of cardiac cell types that often display varying action potential morphologies [5,14].

Efforts to improve cardiac differentiation protocols are also influenced by the need for better cardiac models for safety pharmacology testing. The S7B guidelines from the International Conference of Harmonisation (IHC) stipulate a need to investigate ion channel interactions, in particular with hERG receptors [15]. These guidelines encourage simple studies, often with Chinese hamster ovarian (CHO) cells transfected with a hERG receptor that demonstrate a simplistic and impractical example of ion channel interactions that don't account for the broad range of available ion channels of a functional adult cardiomyocyte [16,17]. These studies also highlight the limited representation of biomimetic systems as pharmacological agents that pass these trials and can later be removed from the market, such was the case with Cisapride [18], and Terfenadine [19] for unknown ion channel interactions not found during pre-clinical testing. The other side of this coin is that beneficial compounds that could help millions of patients, could unfairly be removed from further testing due to an incomplete picture of ion channel interactions in hERG receptor models [20]. The Comprehensive in-vitro Pro-arrhythmic assay (CiPA) is a movement that is encouraging the use of alternative methods including PSC-CM in safety pharmacology testing [20,21]. Commonly PSC-CM represent immature cardiomyocytes similar to embryonic cardiac tissue with an unorganized ultrastructure and poor ion channel presentation which can vary with increased incubation periods leading to inconsistent results [22]. Before PSC-CM become a viable cardiac model for safety pharmacology testing, or to be used in cell therapies, variability in maturation and electrophysiological responses need to be standardized.

Several modern protocols have a range of achievements in meeting the purity and quality guidelines for PSC-CM [10,23–25]. The majority of these protocols focus on the utilization of small molecules responsible for guiding lineage pathways that would be most favourable for producing cardiomyocytes whilst microenvironmental cues of the extracellular matrix, have received less attention. While these chemical signals are important factors, they often lead to unguided differentiation towards a cardiac lineage without the ability to direct chamber specification. Several studies have claimed to enrich kinetic or electrophysiological properties of chamber-specific cell types that are often described as "atrial-like, ventricular-like, and nodal-like" cells [26–29]. However, to consistently produce these chamber-like cell types, specific differentiation protocols need to be developed to direct chamber specificity with rigorous selection criteria that factor in the importance of extracellular matrix proteins (ECMP) [30–32].

The importance of ECMP in cardiac differentiation and maturation is evidenced by the variability of expression in a developing embryo [33]. Furthermore, congenital diseases responsible for improper ECMP expression show the significance ECMP can have on alignment [34], growth [35], morphology [36–38], chamber specification [39,40], and maturation [41,42]. ECMP remodelling following an ischemic event or during progressive heart failure is also evidence of the importance of how cardiomyocytes will adapt to alterations in the ECMP structure [43–46]. Studies utilising decellularised ECMP scaffolds show the influence the ECMP structure can have on inducing differentiation of stem cells towards a cardiomyocyte lineage without the need to implement a differentiation protocol [47–50]. The evidence of these studies into the ECMPs importance during the early stages of cardiomyogenisis shows how providing "outside-in" signaling can augment differentiation [51]. Early methods for culturing hESC used MEF feeder layers that would deposit a complex mixture of ECMP that provided a suitable substrate that allowed attachment whilst maintaining the stemness and proliferation of the cells [52]. More modern protocols now utilize commercial substrates like Matrigel™ or Geltrex™ which are extracted and purified substrates made up of the same complex mixture of ECMP. Whilst these animal-derived matrices have gained a good reputation for maintaining stem cells, they can often show wide variability in composition and do not reflect the native ECMP composition found in cardiac tissue and are a poor representation of the ECMP present during human cardiac development [53,54].

In recent years, considerable work has been devoted to replacing Matrigel with singular ECMP such as fibronectin, laminin or vitronectin [55–58], as well as combinatorial assessments of ECMP matrices [59–61] for the maintenance of stem cell pluripotency. Alternative studies have been investigating protein combinations to direct cardiomyocyte lineage specification by utilizing proteins prevalent in native cardiac tissues such as fibronectin and laminin. Jointly these proteins showed an improved differentiation efficiency when cultured on a 70:30 ratio of fibronectin to laminin [62]. More recent research focuses on identifying specific proteins required for the in vivo maintenance of human cardiomyocytes. The abundance of laminin 221 and 521 in the adult human heart was investigated and showed improved cardiomyocyte progenitor specification and enhanced cardiac function in mice when transplanted into areas of the induced infarct [63]. Other studies demonstrate a strategy for the maturation of hPSC-CM monolayers, by emphasizing the importance of specific ECMP conditions in a 3D culture format and the involvement of integrin signaling pathways in the maturation process [64]. While these findings are intriguing, a comparative analysis with modern differentiation protocols reveals lower differentiation efficiency or improvements when PSC-CM are cultured using specialized techniques and fabricated platforms not readily available to most laboratories. Additionally, the observed enhancement in animal models is often associated with cultures undergoing prolonged in vitro incubation. Conflicting studies suggest that improvements during in vivo cell therapies may arise due to in vitro extracellular matrix remodeling resulting from extended culture periods [64,65], and similar results can be achieved through alternate techniques that do not utilize ECMP substrates [66]. Despite these advancements, the precise role of specific proteins in guiding differentiation, maturation, and chamber specificity within the cardiac lineage remains to be fully understood.

In this paper, we report an ECMP microarray approach to evaluate the role of initial matrix conditions in directing cardiac differentiation in hESCs. We used 6 commonly found ECMP including collagen 1, collagen 3, collagen 4, fibronectin, laminin, and vitronectin by presenting them alone and in combinations to produce 63 different protein permutations. These ECMP surfaces were assessed for promotion of proliferation, maintenance of pluripotency, and expression of germline-specific biomarkers. We then analysed this data in combination with the biomarker expressions that would typically follow cardiomyocyte differentiation by investigating the commitment to the mesoderm linage, and the influence on promoting cardiomyocyte progenitors. Induction of differentiation using media formulations and analysis of cardiomyocyte biomarkers revealed ECMP combinations that enhance cardiomyogenisis, with three surfaces that promote high functional maturation as determined by contraction analysis. Custom criterion – based on molecular markers and action potential morphology –was used to identify ECMP combinations that direct differentiation to ventricular, atrial, and nodal phenotypes, providing the first matrix-based approach to direct chamber specificity whilst highlighting how ECMP affect the critical milestones throughout cardiomyocyte differentiation. The workflow of these experiments are detailed in Fig. 1.

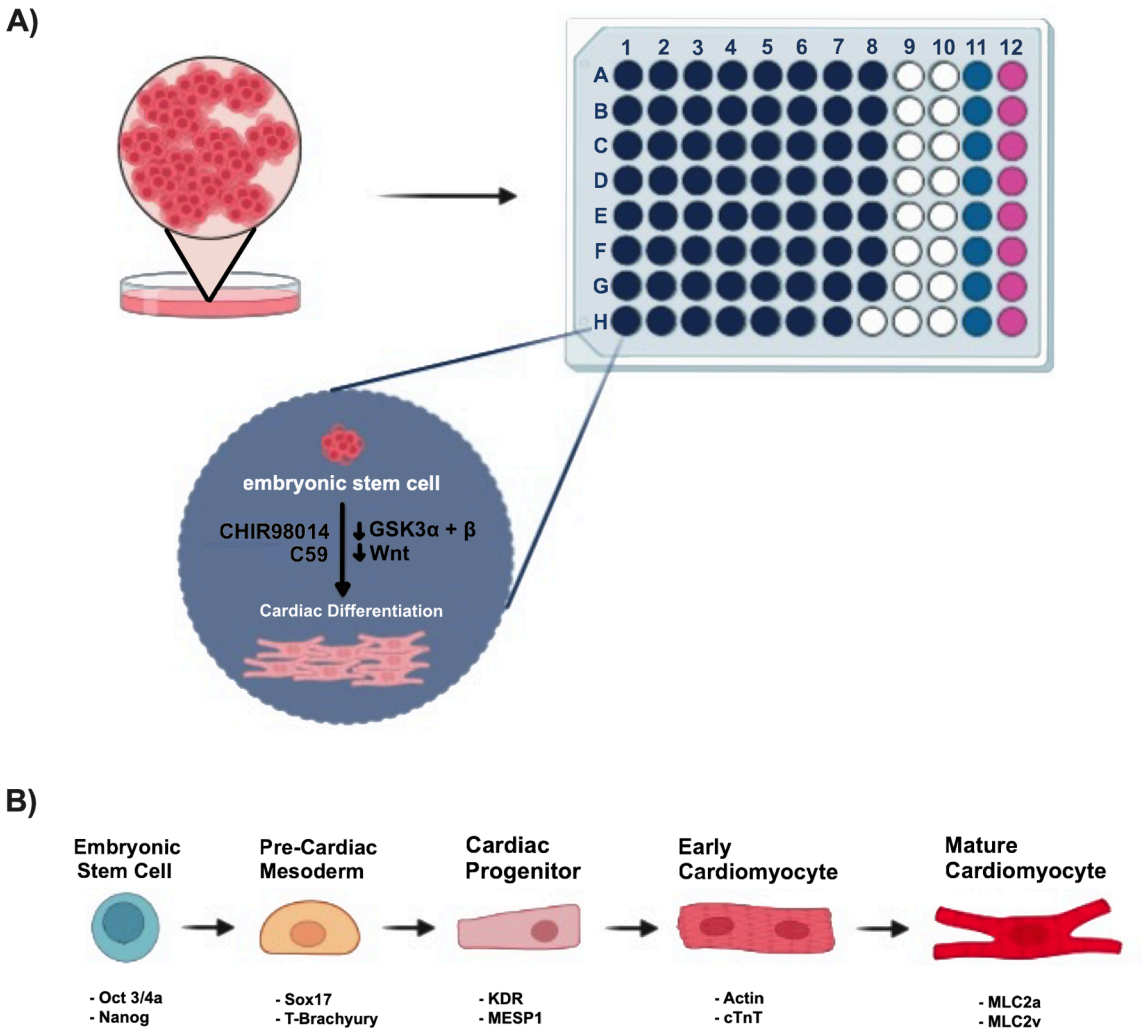

Fig. 1. ECM Array Plate to investigate cardiomyocyte differentiation lineage specification. A) ECMP array seeded with hESC and cultured for 5 days. Cells are then differentiated using a ventricular cardiomyocyte differentiation protocol. B) Cells are fixed and stained at various timepoints throughout the cardiomyocyte lineage so assess the effects ECMP combinations have on differentiation potential. Created by BioRender.com.

Results

Protein microarrays identify optimal microenvironments for pluripotent stem cell proliferation

Before delving into the impact of ECMP on cardiomyocyte differentiation, our investigation first focused on how our ECMP array could affect the proliferation and pluripotency of hESC. To explore the combinations of ECMPs available for supporting pluripotent stem cells, numerous studies have employed an array technique. These studies often utilize protein spotters on a biomimetic hydrogel to enhance throughput, ensuring accuracy and reproducibility. However, caution is warranted, as many of these studies may be misleading, deviating from traditional culture techniques and introducing features that can specifically impact differentiation. Such features include alterations in substrate stiffness [67–69], topographical confinement [70–72], restricted cell populations [72,73], and paracrine signalling from adjacent microenvironments [74,75]. The array spot method, with its incorporated features, may identify optimal ECMP combinations for a particular array setup, but potentially lacks a full representation of the traditional in vitro culture conditions utilized for pluripotent stem cell proliferation and maintenance in clinical settings. Traditional cell culture methods, like plastic multiwell cell culture dishes, are frequently adapted and scaled up for clinical protocols. In contrast, the array-based approach allows the creation of numerous cost-effective and user-friendly microenvironments that can be replicated in various laboratories.

In this study, six commonly encountered ECMP were selected and arranged within a 96-well plate, creating 63 distinct permutations. The chosen matrix proteins included collagen 1, collagen 3, collagen 4, fibronectin, laminin, and vitronectin. Fig. 2A outlines the arrayed protein combinations, utilizing 63 wells of a 96-well plate to represent unique protein permutations. Prior to the fabrication of the array, the proteins were dissolved in 1x DPBS at a concentration of 25 μg/mL. A final volume of 200 μL was added to each well, and the concentrations of individual proteins were adjusted based on the number of proteins combined in each well. This method of concentration dilution was implemented to ensure uniform protein concentrations across all wells, eliminating it as a potential source of variability among combinations.

After seeding hESCs across the array, we measured confluency on each ECMP combination over 5 days using the Olympus Confluency Checker. For measuring cell viability, alamarBlue™ was used as a measure of cells' metabolic activity. This was used in conjunction with the confluency software to differentiate between growth and fitness. From Fig. 2C and S1, we can see a general correlation between cell viability and confluency for most ECMP combinations but also some disparities. This highlights the dynamic nature of hESC in response to different microenvironments and how cell spreading is not always correlated to the cell's metabolic fitness and vice versa. The dotted

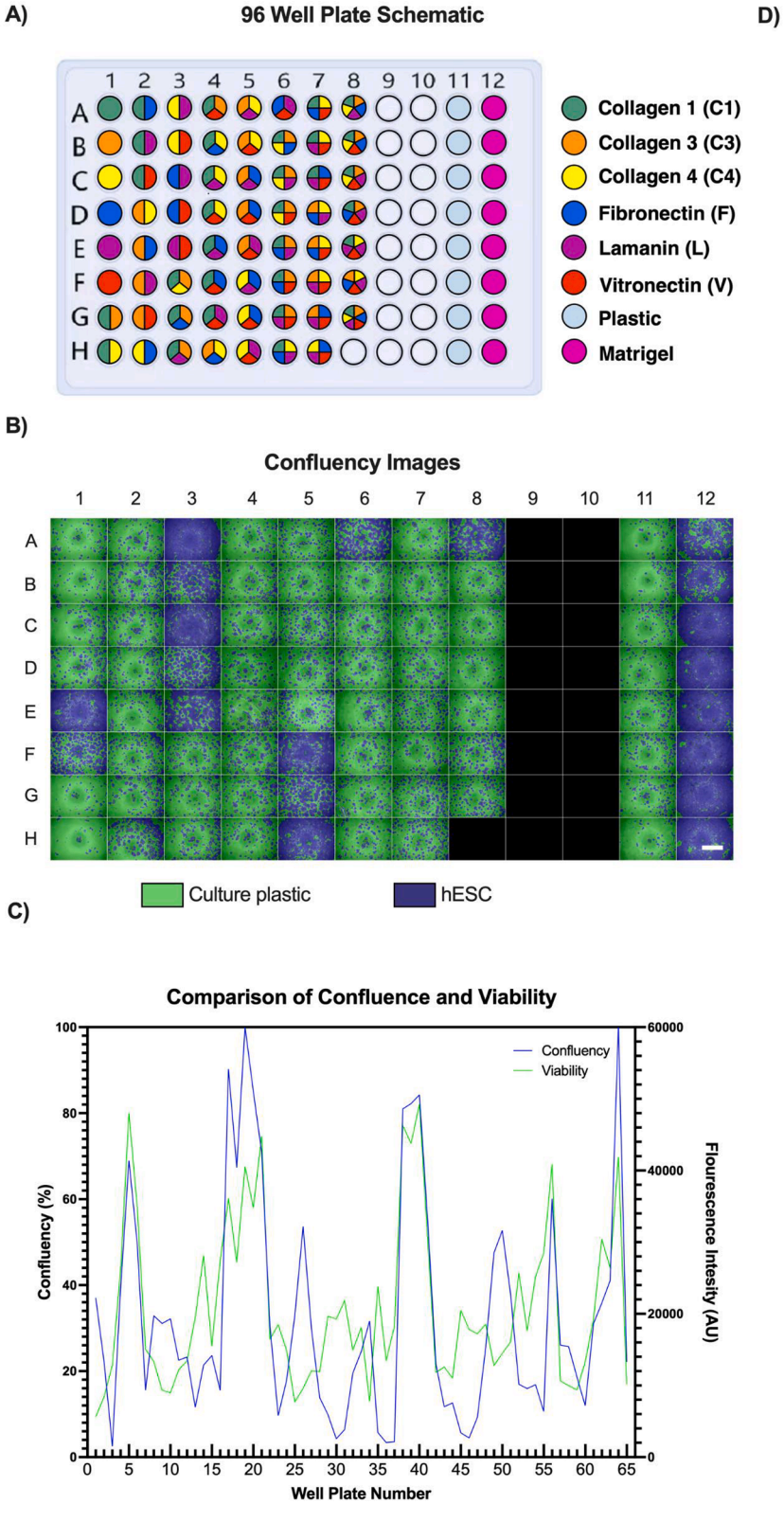

D)

Protein Combination	Well plate Location	Well Plate Number
C1	A1	1
C3	B1	2
C4	C1	3
F	D2	4
L	E1	5
V	F1	6
C1C3	G1	7
C1C4	H1	8
C1F	A2	9
C1L	B2	10
C1V	C2	11
C3C4	D2	12
C3F	E2	13
C3L	F2	14
C3V	G2	15
C4F	H2	16
C4L	A3	17
C4V	B3	18
FL	C3	19
FV	D3	20
LV	E3	21
C1C3C4	F3	22
C1C3F	G3	23
C1C3L	H3	24
C1C3V	A4	25
C1C4F	B4	26
C1C4L	C4	27
C1C4V	D4	28
C1FL	E4	29
C1FV	F4	30
C1LV	G4	31
C3C4F	H4	32
C3C4L	A5	33
C3C4V	B5	34
C3FL	C5	35
C3FV	D5	36
C3LV	E5	37
C4FL	F5	38
C4FV	G5	39
C4LV	H5	40
FLV	A6	41
C1C3C4F	B6	42
C1C3C4L	C6	43
C1C3C4V	D6	44
C1C3FL	E6	45
C1C3FV	F6	46
C1C3LV	G6	47
C1C4FL	H6	48
C1C4FV	A7	49
C1C4LV	B7	50
C1FLV	C7	51
C3C4FL	D7	52
C3C4FV	E7	53
C3C4LV	F7	54
C3FLV	G7	55
C4FLV	H7	56
C1C3C4FL	A8	57
C1C3C4FV	B8	58
C1C3C4LV	C8	59
C1C3FLV	D8	60
C1C4FLV	E8	61
C3C4FLV	F8	62
C1C3C4FLV	G8	63
Matrigel	A11-H11	64
Plastic	A12-H12	65

Fig. 2. ECMP Plate Array A) Layout of arrayed ECMPs in a 96 well plate. hESC are seeded at $1.24x10^4 cells/cm^2$ to allow proliferation over 5 days. **B)** Images of hESC using Olympus confluency checker where green donates culture plastic and purple denotes cells. Images taken on day 5 at 10X magnification, Scale bar 500 μM. **C)** Graphical comparison of the viability and confluency of all 63 ECMP combinations to highlight similarities and differences of the ECMP combinations on the hESC. **D)** List of protein combinations used to generate the ECMP array with the proteins name abbreviation, the location of the well in the 96 well plate and the well plate number referenced to the X axis of the comparison of confluency and viability graph.

threshold lines in Figure S1 indicate the response of hESC on the commercial substrate Matrigel. We see there are a handful of ECMP combinations that had higher confluency and metabolic viability in comparison to Matrigel, indicating an improved proliferative ability on select ECMP combinations. Most ECMP combinations showed a decreased confluence and viability compared to Matrigel, indicating some ECMP combinations can inhibit cell proliferation while others may display an induced apoptotic response. This comparison demonstrates how hESC morphology is not always the best indicator of viability.

On day 5 (120 h), three independent cultures of hESC cells from the 63 different ECMP combinations were fixed and stained with DAPI to assess the quantity of DNA present in each well (PRO):

$$PRO = \frac{\chi - \mu_{DNA}}{c} \quad (1)$$

Where χ is the Log_2 of the DNA signal for the well, μ_{DNA} is the average of the Log_2 DNA signal for all the wells on the plate, and σ_{DNA} is the standard deviation of the Log_2 DNA signals for all the wells on the plate. Proliferation Index values from the replicated cultures (n = 3 per ECMP condition) were averaged for each ECMP combination (μ_{PRO}). The proliferation behaviour of the hESC cells to each ECMP combination, μ_{PRO} are displayed in a heat map in Fig. 2. Each row corresponds to the ECMP combination, and the three columns represent the three independent cultures. The rows and columns were clustered using Euclidian distancing as a similarity metric with an average linkage method. The combinations are displayed using a color code of blue to red to indicate two cluster groups of lower and higher proliferation compared to the global average mean ($\mu_{PRO} = 0$), respectively.

By performing a Pearson correlation between the three independent cultures, we investigated the prevalence of ECMP combinations in relation to the observed proliferation. We found a number of ECMP combinations that consistently produced high proliferation rates (red) and low proliferation rates (blue) as displayed in Fig. 3. Whilst these ECMP combinations could be prevalent in these groups due to biological variation, the prevalence of the individual ECMP in the high and low proliferation combinations is intriguing. These findings are also mirrored in Figure S4 where the effects of the individual ECMP on proliferation when averaging from the three biological repeats.

Prior research has emphasized the significant role of collagen 4 as a major component of the basement membrane across the human body, often collaborating with various extracellular matrix (ECM) proteins to promote growth and remodeling in disease scenarios [45]. Therefore, it is not surprising that our findings indicate an equal presence of collagen 4 in both high and low-proliferation groups. As illustrated in Fig. 3, S2, and S4, laminin and vitronectin are prominently featured in the high proliferation group but less so in the low proliferation group. Conversely, collagens I and III exhibit a higher frequency in the low proliferation group and a lower frequency in the high proliferation group.

Relationships between proliferation and pluripotency on defined protein microenvironments

To ascertain the effects of the ECMP combinations on the level of pluripotency in comparison to proliferation, hESCs were cultured for 5 days before being fixed and stained for stemness markers OCT3/4a and Nanog (Fig. 4). While OCT3/4a and nanog will normally be highly expressed in pluripotent cells, the expression level of nanog can be variable in individual cells. Previous studies on pluripotency in hESC have also shown that a low nanog expression level can maintain pluripotency in culture without differentiating [106]. Whilst we expect stemness markers in hESC to be highly expressed in undifferentiated cells, we used the expression of OCT3/4a as a measure of pluripotency and confirmed pluripotency by comparison to the nanog expression level. For each protein combination, the ratio (R) of the Log_2 of the OCT3/4a signal and the DNA signal was calculated. From this, a pluripotency index value (PLU) can be calculated for each protein combination using the equation below:

$$PLU = \frac{R - \mu_{ratio}}{\sigma_{ratio}} \quad (2)$$

Here, R represents the ratio value for the protein combination, μ_ratio signifies the average of all ratio values across every protein combination, and σ_ratio is the standard deviation for all ratio values across every protein combination. Each ECMP combination is then assigned coordinates (PRO, PLU) to visualize the relationship between hESC proliferation and pluripotency on different ECMP combinations (Fig. 4B). Pluripotency index values from three independent replicates (n = 3 per ECMP condition) were collected and averaged (μ_PLU) for each ECMP combination.

In Figure S3, the heatmap displays individual pluripotency index values alongside proliferation index values. Rows represent different ECMP combinations, and the six columns represent independent proliferation and pluripotency array experiments. Clustering analysis, utilizing Euclidean distancing and an average linkage method, organized ECMP combinations into four distinct groups, aligning with the quadrants in Fig. 4B. These groups are: i) high proliferation and high pluripotency (red group/top right), ii) high proliferation and low pluripotency (green group/bottom right), iii) low proliferation and low pluripotency (blue group/bottom left), and iv) low proliferation and high pluripotency (orange group/top left).

Plotting the coordinates (PRO, PLU) uncovered a negative correlation between pluripotency and proliferation index values ($r = -0.7847$, $p < 0.0001$), suggesting that an ECMP reducing pluripotency tends to increase proliferation. No ECMP combinations strongly promoted both proliferation and pluripotency simultaneously. However, combinations including collagen I (C1) and collagen IV (C4) with laminin (L) or vitronectin (V) emerged more than once as promoters of both. Conversely, the absence of collagen IV (C4) in these combinations led to decreased pluripotency and proliferation. Matrigel favored proliferation over pluripotency at day 5, possibly due to slight differentiation from high confluency. A repeated test on Matrigel fixed on day 3 showed the expected result of high pluripotency and lower proliferation. Examples of proteins dominant in each quadrant are illustrated in Fig. 4A with OCT3/4 immunostaining images.

Correlation plots in Figure S4 analyze the magnitude effects of each ECMP on proliferation and pluripotency. Collagens 1, 3, and 4 had a negative impact on proliferation but a net positive effect on pluripotency, indicating a conducive environment for maintaining stem cells. Collagen 4 had a minor impact on proliferation compared to collagens 1 and 3. This effect is also observed in Fig. 4 between the blue and red quadrants, where the ECMP combinations containing collagen 4 had higher pluripotency. Collagen 1 had the most significant impact, decreasing proliferation and promoting pluripotency. Laminin and vitronectin positively affected proliferation but had a net negative impact on pluripotency, suggesting a conducive proliferative microenvironment with differentiation influence. Fibronectin was the only ECMP negatively affecting both proliferation and pluripotency, and no ECMP showed a positive impact on both.

Defined matrix proteins guide the expression of germline molecular markers

The ability to generate all cell types from a single hESC means we have the opportunity to develop cardiac models and specific cardiac cell types that could be used for regenerative cell therapies. The utilization of an ECMP substrates is allowing us to manipulate hESC differentiation and guide them down specific pathways. Insights into embryology have revealed key signaling pathways that regulate germline specification that can also influence the formation of their downstream derivatives.

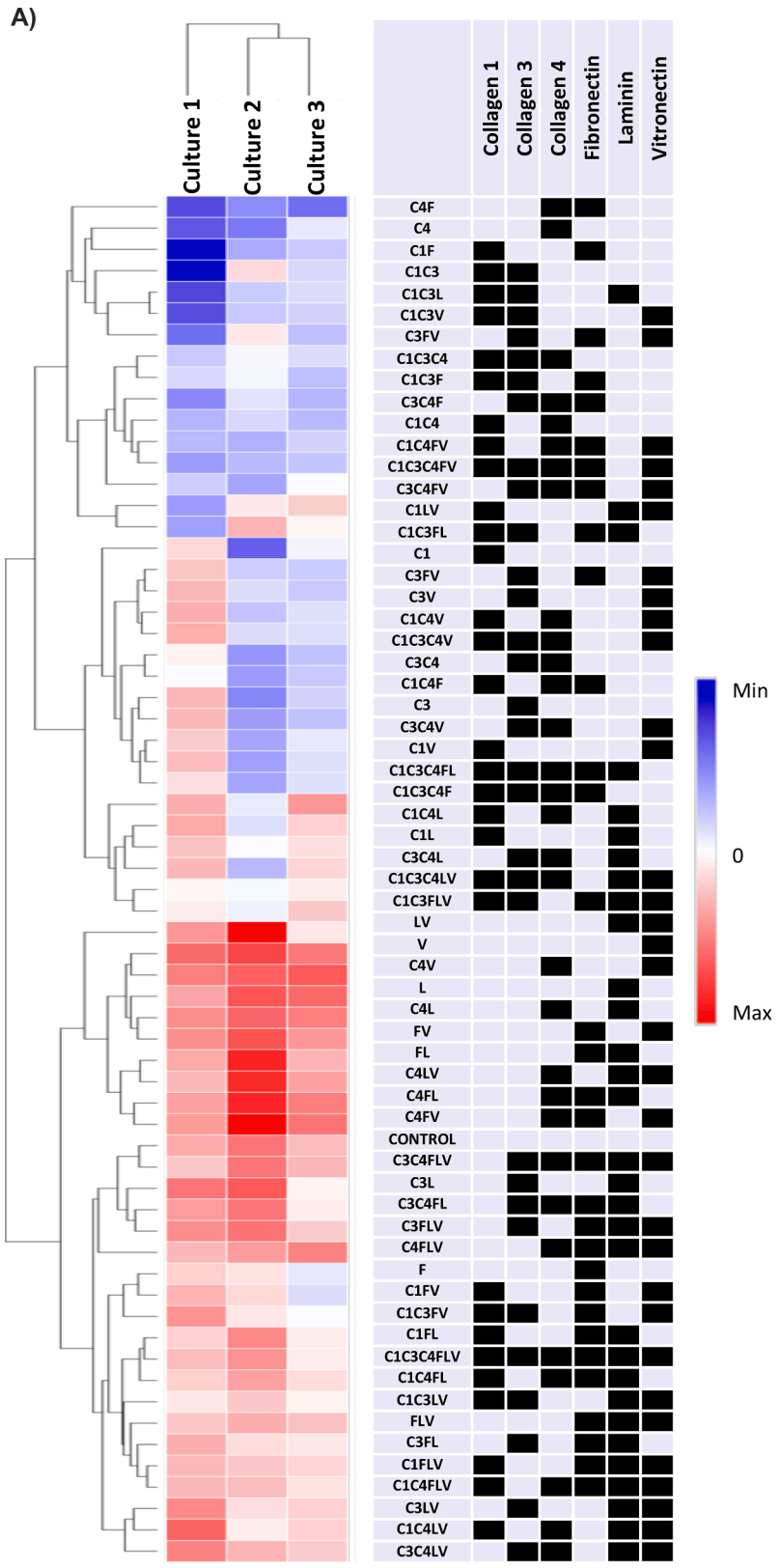

B)

Low proliferation ECMP

	Protein Combination
1	C4
2	C1C4
3	C1F
4	C3C4
5	C4F
6	C1C3C4
7	C1C3F
8	C1C3L
9	C1C3V
10	C1C4F
11	C3C4F
12	C1C3C4L
13	C3C4FV
14	C1C3C4FV

Protein	# of groups including protein
Collagen 1	9
Collagen 3	9
Collagen 4	10
Fibronectin	6
Laminin	2
Vitronectin	3

C)

High proliferation ECMP

	Protein Combination
1	Matrigel
2	L
3	V
4	C4L
5	C4V
6	FL
7	FV
8	LV
9	C3FL
10	C3LV
11	C4FL
12	C4FV
13	C4LV
14	FLV
15	C1C4FL
16	C1FLV
17	C3C4LV
18	C3FLV
19	C4FLV
20	C1C4FLV
21	C3C4FLV

Protein	# of groups including protein
Collagen 1	3
Collagen 3	5
Collagen 4	10
Fibronectin	12
Laminin	15
Vitronectin	14

Fig. 3. Heat map of extracellular matrix protein (ECMP) combinations effect on human embryonic stem cell (hESC) proliferation. A) Heat map of the mean proliferation index values (μ_{PRO}) of each ECMP combination (row) for the three independent cultures (columns). The ECMP combination are indicated with the protein name acronym and the shaded boxes in the table to the right of the heat map. A hierarchical clustering was performed with a Euclidian distancing metric and an average linkage method. Hierarchical clustering of the ECMPs revealed two segregated groups (i) Higher proliferation than the global average mean (red boxes) (ii) Lower proliferation than the global average mean of 0 (blue boxes). **B and C)** listed ECMP combinations that produce a consistently higher or lower proliferation response in three independent cultures. A secondary breakdown of the frequency of individual ECMP in the high and low proliferation combinations is also listed.

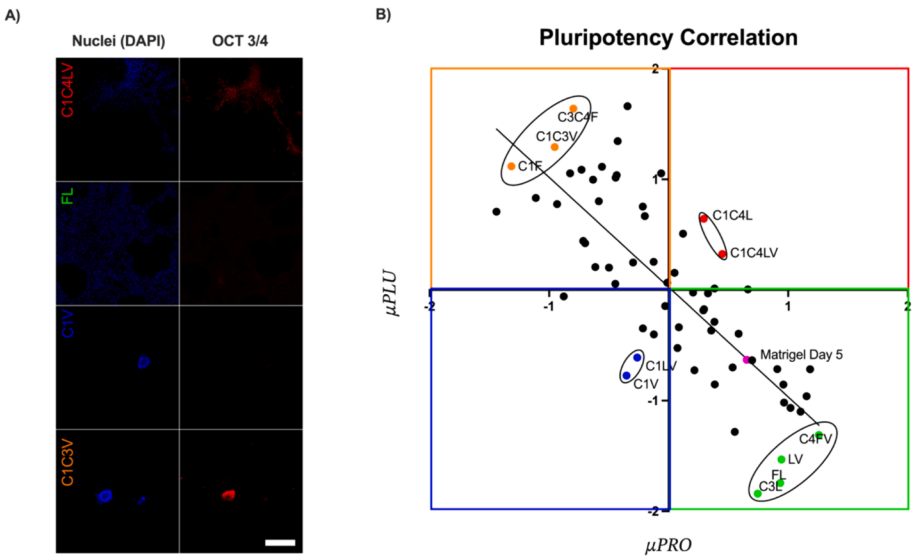

Fig. 4. Influence of extracellular matrix protein (ECMP) combinations on human embryonic stem cell (hESC) proliferation and corresponding pluripotency on day 5 of culture. A) Immunofluorescence images of the DAPI and OCT4 biomarker at 10X magnification (Scale bar = 100μ*M*). These images are representative of similar images (n = 3) using a single plane confocal image. B) The mean proliferation index values (μPRO) and mean pluripotency index values (μPLU) for each ECMP combination on day 5 of the culture were average between the three independent cultures and graphed using a Pearson's correlation. The ECMP combinations are plotted into one of four groups i) High proliferation and high maintenance of pluripotency (red) ii) High proliferation and low maintenance of pluripotency (green) iii) Low proliferation and low maintenance of pluripotency (blue) iv) Low proliferation and high maintenance of pluripotency (orange). These high and low data points are referring to the averaged index values around the global average mean (0).

Employing our ECMP array for evaluating the impact of ECMP combinations on proliferation and pluripotency in H9 hESC, we discovered that specific ECMP combinations exhibit superior pluripotency promotion compared to leading commercial substrates like Matrigel™ and Geltrex™. Notably, certain ECMP combinations demonstrated diminished expression of pluripotency markers, suggesting potential germ layer differentiation and the potential to direct a specific germ lineage. The ability for ECMP combinations to potentially influence germ linage specification is intriguing as cardiac differentiation could be enhanced if ECMP combinations promote mesodermal and pre-cardiac lineages. Wnt activation is required for the activation of all three germlines but additional regulatory signaling is required for specific germlines. Endodermal and mesodermal lineages originate from a Foxa2 positive region of the primitive streak and require Wnt suppression and activin promotion and are generally able to able to alternate until lineage commitment proteins are expressed (4). To explore this further, we immunostained the hESC for the endoderm marker Sox17 and the mesoderm marker T-Brachyury. Using the equation below, we then used the averaged intensity signals from subsequent con-focal images to create an index value for each of the 63 protein combinations.

$$BiomarkerIndexValue(BIV) = \frac{\chi - \mu_{BIV}}{\sigma_{BIV}} \quad (3)$$

Where the Biomarker Index Value (BIV) is calculated from χ which is the Log_2 of the signal for the well, μ_{BIV} is the average of the Log_2 signal of all the wells on the plate, and σ_{BIV} is the standard deviation of the Log_2 signals of all the wells on the plate. These germ layer index values are averaged from replicated cultures (n = 3) for each ECMP combination and displayed as a final index value for the germ line biomarker (μ_{germ}).

These averaged germ layer indices were subsequently compared to proliferation and pluripotency indices, forming a comprehensive heatmap cluster diagram in Fig. 5A. In the cluster diagram, each row signifies an individual ECMP combination, and columns represent averaged proliferation indices, pluripotency indices (OCT3/4a and Nanog), and germ layer markers (Sox17 and T-Brachyury). Hierarchical clustering, utilizing Euclidean distancing and average linkage, discloses three distinct groups: 1) low pluripotency and high germ layer differentiation, 2) high pluripotency and low germ layer differentiation, and 3) a central cluster displaying non-partisan expression. This clustering effectively highlights the relationship between pluripotency and germ-layer differentiation is broad.

Correlation graphs further illuminate these relationships. Fig. 5B shows a Pearson's correlation graph between Sox17 and T-Brachyury index values indicating a moderate positive correlation (r = 0.4668, R2 = 0.1996, p=<0.0001), suggesting a potential preference for multi-lineage specification when ECMP signals encourage deviation from pluripotency. Due to the index values being calculated from images of multiple cells in a culture well, heterogenous populations of cells expressing endodermal and mesodermal markers is often observed. This correlation graph also shows data points that deviate from the trendline, indicating that some ECMP combinations influence a preference for Sox17 or T-Brachyury expression. Specific ECMP combinations, such as C1C3V, C1C3F, and C3C4, exhibit enhanced Sox 17 and expression and C1, C3, and C4 all showed enhanced T-Brachyury expression (Fig. 5C and S5) signifying ECMPs influence on lineage commitment. Notably, C3C4FLV demonstrates a capability to promote multi-lineage specification by enhancing both T-Brachyury and Sox17 expression.

The hierarchical cluster also revealed distinct groups exhibiting either low pluripotency and high germ layer differentiation or high pluripotency and low germ layer differentiation. A central region, however, remains ambiguous, suggesting co-expression of pluripotency and germ layer markers or uncorrelated expression within the same well. Pearson's correlation between average pluripotency (μ_{Plu}) and germ layer (μ_{germ}), index values establish a moderate negative correlation (r = -0.4104, R2 = 0.1684, p=<0.0001) (Fig. 5D), reinforcing the dynamic interplay between pluripotency and germ layer commitment. These findings provide valuable insights into the nuanced relationship among ECMP combinations, pluripotency, and germ layer differentiation.

Expression patterns of MESP1 and MLC2 isoforms predict optimal cardiomyocyte differentiation

By narrowing the view on these 63 protein combinations, we find

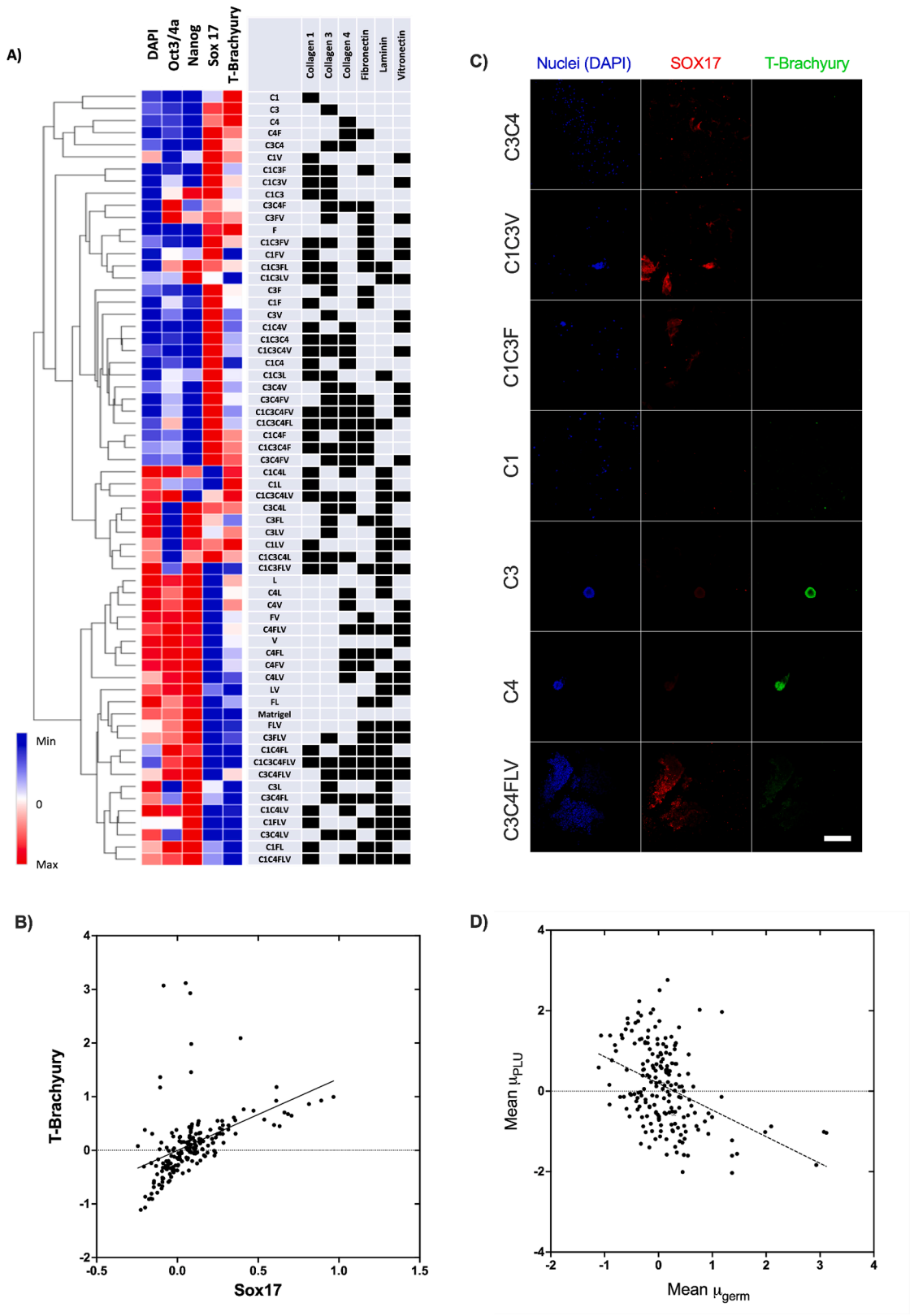

Fig. 5. Heat map of extracellular matrix proteins (ECMPs) combinations effect on human embryonic stem cell (hESC) proliferation, pluripotency, and germ layer differentiation. A) Heat map of the mean proliferation index values (μ_{PRO}), mean pluripotency index values (μ_{Plu}), and mean germ layer index values (μ_{Germ}) for each ECMP combination (row). The ECMP combination is indicated with the protein name acronym and the shaded boxes in the table to the right of the heat map. **B)** Pearson correlation matrix of sox17 and T-Brachyury index values (r = 0.4468 R^2 = 0.1996). **C)** Images showing the high Sox17 and low T-Brachyury expression on C3C4, C1C3V, and C1C3F protein combinations, low Sox17 and high T-Brachyury expression on C1, C3, and C4 protein combinations, and the dual expression of Sox17 and T-Brachyury on C3C4FLV. Corresponding immunocytochemical stain DAPI (blue), Sox17 (Red), and T-Brachyury (green) scale bar is 100 μm. **D)** Pearsons's correlation between the mean pluripotency index values (μ_{PLU}) and the mean germ layer index values ((μ_{Germ}) for all 63 combinations (r = -0.4104 R^2 = 0.1684).

there are specific ECMP combinations that can promote germ layer differentiation while others promote pluripotency. To further probe cardiac lineage specification, we first explored several markers of cardiac progenitors including kinase insert domain receptor (KDR), which is used to signify a pre-cardiac mesoderm cell type [76]. T-Brachyury^{+}/KDR^{+} cells can enter the cardiac lineage and express various genes and transcription factors as the cells become progressively differentiated. The regulation of multipotent cardiovascular progenitor cell specification can be observed through the enhanced expression of mesoderm posterior 1 (MESP1) [77]. After immunostaining and hierarchical clustering analysis of KDR and MESP1 stained populations, alongside the SOX17 and T-Brachyury populations evaluated in the preceding section, we see a range of differential expression across all ECMPs. However, there is no significant correlation between the early germ layer and cardiac progenitor molecular markers (Figure S6-S12). While selecting ECMPs alone may promote germ layer specification and enhance cardiac progenitor markers, we believe that temporal administration of cardiac-promoting supplements is necessary for cardiac differentiation.

To evaluate how protein combinations may trigger cardiac lineage programs, we subjected our cultures to differentiation media conditions and immunostained for T-Brachyury, KDR and MESP1. Fig. 6 shows a cluster diagram constructed from the index values on all 63 ECMP combinations for T-brachyury, KDR, and MESP1 pre and post-differentiation. By performing hierarchical clustering, we can see the segregation of groups that correspond to high and low expression of both pre and post differentiation expression of MESP1, where the majority of the 28 ECMP combinations that showed positive index values for pre- and post-differentiation expression of MESP1 are represented in the bottom half of the cluster diagram. A correlation of MESP1 expression for pre and post differentiation shows a weak positive correlation in Figure S13 ($r = 0.3243$ $R^2 = 0.1052$p=<0.0001). When we isolate the 28 ECMP combinations that had a double positive MESP1 expression for pre and post differentiation, we see a tighter correlation that remains weakly positive ($r = 0.2468$ $R^2 = 0.06090$p $= 0.0264$). This weak correlation is unsurprising because MESP1 expression is transiently expressed throughout differentiation. Nevertheless, it is still feasible that ECMP combinations that show positive expression of MESP1 in both pre and post differentiated cells will produce enhanced differentiation of cardiomyocytes and may positively influence cardiomyocyte maturation.

The indication of maturation is frequently associated with the manifestation of mature cardiomyocyte markers such as cardiac troponin (cTnT) [78]. In the developmental phase of hearts, there is typically a higher demand for strongly contracting cardiomyocytes in ventricular tissue as opposed to atrial tissue due to the resistance and forces needed for effective blood ejection into the body. These two chambers develop alternate versions of the myosin light chains (MLC) denoted MLC2a and MLC2v. This transition is commonly associated with maturation in in-vitro cultures where the immature cardiomyocytes predominantly express the MLC2a gene, which undergoes a switch to the MLC2v isoform during maturation [79–82,102]. It has since become standard practice to represent the expression of MLC2a to MLC2v as a comparison of maturation between groups where more matured groups display more MLC2v and less MLC2a [83,107]. To assess the maturation of the cardiomyocytes differentiated on our 63 protein combinations, we immunostained our cells for cTnT, MLC2a, and MLC2v on day 14 of the differentiation protocol and used the equation previously used (equation (3) to generate index values for the cardiomyocyte maturation biomarkers.

These index values are averaged from replicated cultures ($n = 3$) for each ECMP combination (μ_{CMAT}). These averaged CMAT index values are compared to the proliferation, pluripotency, germline, and cardiac progenitor index values and are displayed in a heatmap cluster diagram in Fig. 6. Hierarchal clustering shows that the double positive MESP1 ECMP combinations grouped in the lower half of the cluster diagram all show positive MLC2v expression, with the majority showing a strong negative MLC2a expression.

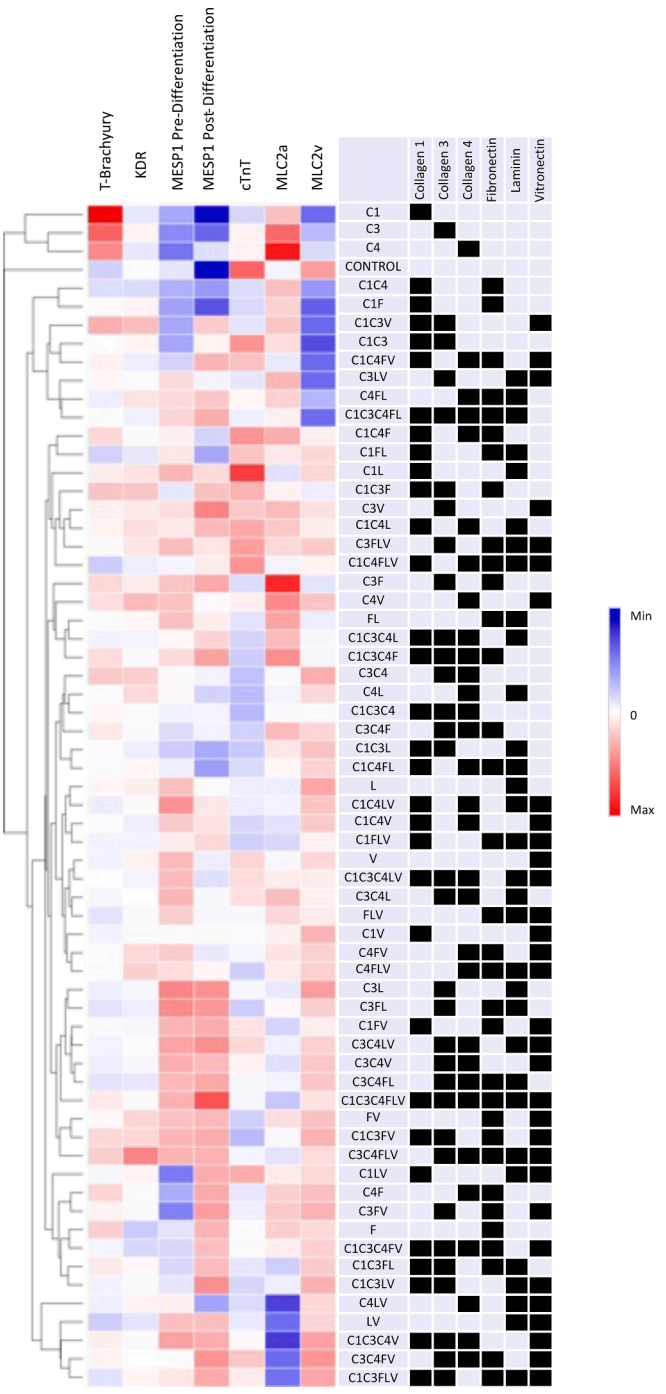

Fig. 6. Extracellular matrix protein (ECMP) combinations effect on human embryonic stem cell (hESC) germ line, cardiac progenitor, and mature cardiac biomarker expression. Heat map of average expression index values for each biomarker (column) on the individual ECMP combination (rows). Three independent array cultures were conducted for each biomarker. The ECMP combination is indicated with the protein name acronym and the shaded boxes in the table to the right of the heat map. A hierarchical clustering was performed with a Euclidian distancing metric and an average linkage method. High (red) and low (blue) data points are referring to the averaged index values around the global average mean (0).

Surprisingly only a few shows positive cTnT expression in this same group. When looking at the cTnT expression, only two ECMP combinations show negative MLC2v expression suggesting that expression of cardiac troponin leads to the progressive maturation of cardiomyocytes.

We expect to see a positive correlation when we compare the MESP1 expression for both pre and post-differentiation to these mature cardiac markers. Figure S13 shows this correlation of MESP1 with cardiac troponin, where no correlation is observed in both the pre and post differentiation MESP1 expression graphs, and the correlation of MLC2a with MESP1 for both pre and post differentiation. In both these graphs, we see a weak negative correlation, as expected. We would assume that expression of MESP1 would correlate with cardiac differentiation and maturation; thus, as MESP1 expression increases, we would see enhanced cardiac differentiation and a decrease in MLC2a expression. There is a positive correlation between MESP1 pre and post differentiation expressions with MLC2v, supporting the hypothesis that increased expression of MESP1 often leads to enhanced differentiation and maturation of cardiomyocytes as dictated by increased expression of MLC2v (Figure S14).

Select matrices that promote cardiomyogenisis and influence chamber specification

Following the completion of various biomarker stains and the

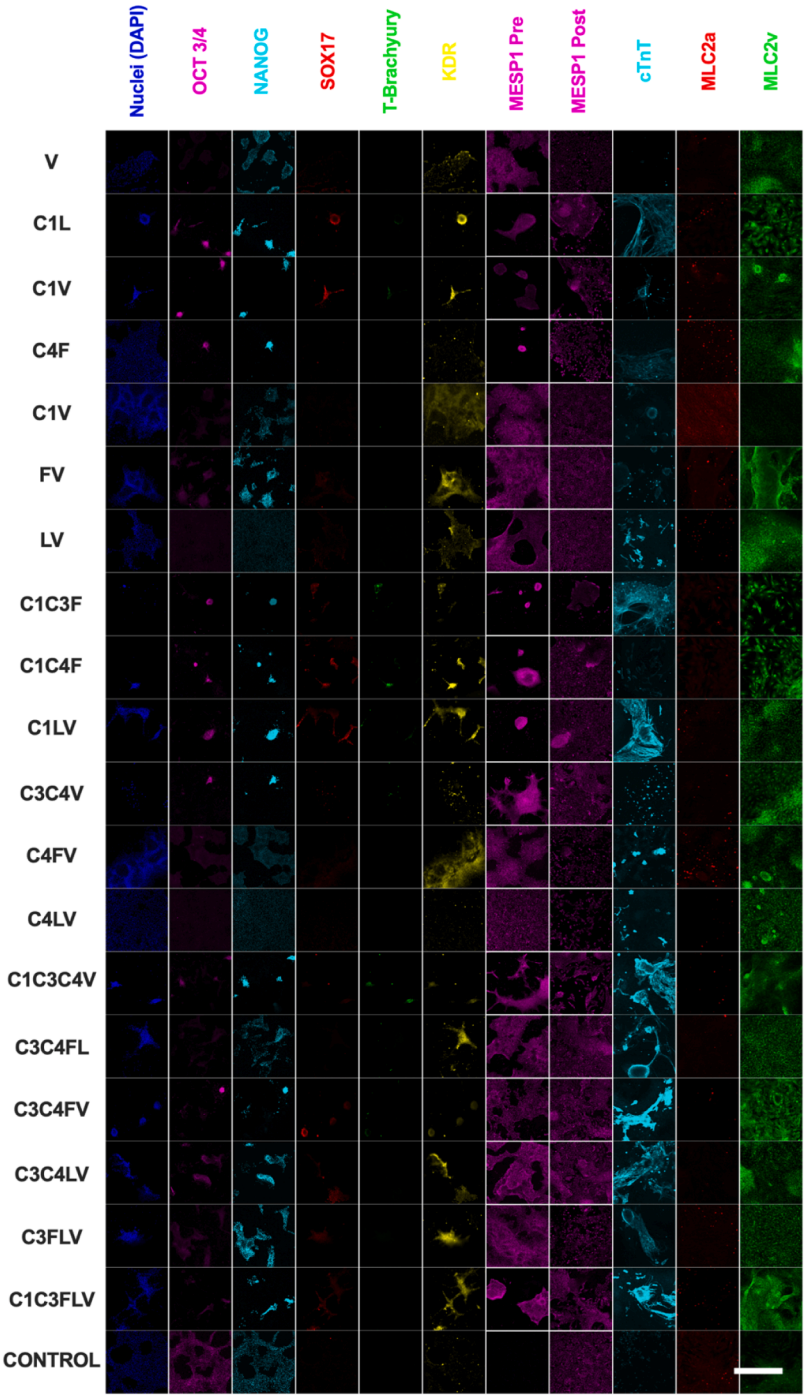

Fig. 7. Confocal images of extracellular matrix protein (ECMP) combinations effect on human embryonic stem cell (hESC) expression of pluripotency, germ line, cardiac progenitor, and mature cardiac biomarkers. Immunofluorescence images of stains DAPI (blue), Oct3/4a (Magenta left) Nanog (cyan Left) Sox17 (red left), T-Brachyury (green left) KDR (yellow), Mesp1 Pre and Post differentiation (Magenta center), and cTnT (cyan right), MLC2a (red right), MLC2v (green right), scale bar is 100 μm.

examination of the impact of ECMP combinations on the expression of cardiac progenitor and maturation markers, our focus shifted to identifying the ECMP substrates capable of generating functional contracting cardiomyocytes. Out of the 63 protein combinations tested, along with the Matrigel control group, 20 exhibited the presence of contracting cardiomyocytes. Fig. 7 displays confocal images depicting the observed biomarker stains for each of these 20 ECMP combinations.

Given the extensive collection of confocal data, we thought it appropriate to conduct a principal components analysis (PCA) to explore potential clustering among the ECMP combinations that induced contracting cardiomyocytes compared to those that did not. In Fig. 8, the PCA graph displays all 63 protein combinations and the Matrigel control groups in triplicate. Although a slight clustering effect of ECMP combinations resulting in contractions is observed on the left side of the graph, it is not distinctly separated from the non-contracting group. The principal components primarily contributing to the separation of the contracting from the non-contracting groups are MESP1 (both pre and post differentiation) and MLC2v. Moreover, groups such as pluripotency, T-brachyury, and MLC2a are crucial for distinguishing non-contracting groups (Figure S15B). When evaluating the supporting graphs for the PCA plot (Figure S15C and D) we found it to be the wrong choice for distinguishing differences between the contracting and non-contracting groups. As this plot does not clearly distinguish between the two groups, we explored an alternative dimension-reduction method called t-distributed stochastic neighbouring embedded (t-SNE). Fig. 8B shows the t-SNE graph for all 63 ECMP combinations and the control group, offering a visual representation of potential clusters with distinct characteristics. While t-SNE is not a statistical tool, it color-codes ECMP combinations according to contracting and non-contracting groups, revealing a significant crossover between the two. Unlike PCA plots, t-SNE displayed a distinct tight cluster of contracting cells separated from the main data body (highlighted with a circle). To account for variable parameters, we produced the same cluster plot with different perplexity values (0–50), that consistently showed the same small tight cluster of contracting cells (Figure S16). This suggests that the ECMP combinations within this cluster had unique values setting them apart from other contracting and non-contracting data points. The ECMP combinations in this cluster—C1C3FLV, C3C4FV, and C1C3C4V—stand out in the cluster diagram (Fig. 6), grouped at the bottom, indicating similarities in the expression of mesoderm, cardiac progenitor, and cardiomyocyte maturation markers. Notably, the MESP1 post-differentiation and MLC2v index values are highly expressed above the global average mean in these three ECMP combinations.

Upon identifying three distinct ECMP groups (C1C3FLV, C3C4FV, and C1C3C4V) that formed a separate cluster from the main dataset, we conducted a series of a-priori statistical tests to determine if these three groups exhibited statistically different biomarker expressions compared to the control group on Matrigel™. The null hypothesis stated that all biomarker expressions in hESC were equal when cultured on Matrigel™ and the three specified ECMP combinations. To assess the statistical significance of any differences, we employed a MANOVA test, allowing for the examination of multiple variables. The selected biomarkers for this analysis were T-brachyury, KDR, MESP1, cTnT, MLC2a, and MLC2v. These biomarkers were chosen due to their relevance in highlighting key stages of cardiomyocyte lineage specification, encompassing germ layer differentiation, cardiac mesoderm, cardiac progenitor, and mature cardiomyocyte protein expression. The MANOVA test yielded a significant difference among the four groups, as indicated by a Pillai's Trace value of 2.5068, $F(18, 15) = 4.2354$, and $p = 0.0035$. Consequently, we reject the null hypothesis, concluding that there is a significant disparity in biomarker expression levels between the Matrigel™ and ECMP combinations. Further details on these statistical tests are available in the supporting methods.

Next, we sought to explore the contractile properties of these differentiated cells to examine the early-stage changes in the contraction profile. This was achieved with high-speed optical mapping of the contracting cardiomyocytes that are then analyzed using Pulse Video Analysis software from CuriBio [84]. The electrophysiological and kinetic characteristics of cardiomyocytes serve as essential indicators for identifying chamber specification based on the action potential (AP) morphology. Distinct cardiac cell types exhibit unique ways of propagating the action potential [5,14,29]. While textbook definitions exist for these chamber-specific action potential morphologies, practical observations often reveal a spectrum of morphologies both in vivo and in vitro. This variability can be attributed to factors such as the chosen location to measure the electrophysiological activity in the heart or the presence of multiple cell types within the same culture dish. Notably, atrial, and ventricular waveforms exhibit a range of morphologies when measured from different locations or at different depths within the heart wall [85,86].

Despite these variances, we have tried to develop a template criterion that could be used to identify chamber-specific AP morphologies

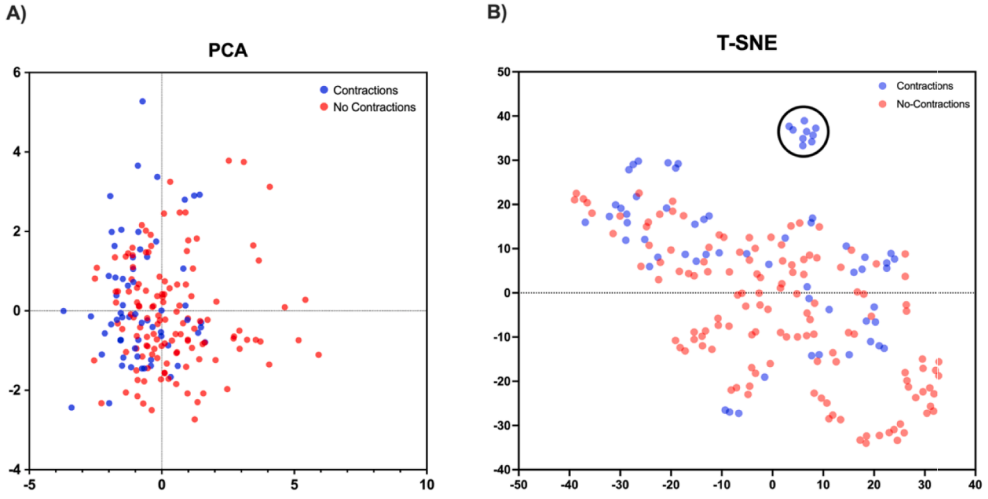

Fig. 8. Principal component analysis (PCA) and T-distributed stochastic neighbor embedding (T-SNE) of biomarker index data from hESC cells on 63 ECMP combinations and a Matrigel control group. A) Data points are separated into two groups, the ECMP combinations that produced contracting cardiomyocytes (blue dots) and those ECMP combinations where no cardiomyocytes were observed contracting (red dots). B) t-distributed stochastic neighbor embedding plot. Data points are separated into two groups, the ECMP combinations that produced contracting cardiomyocytes (blue dots) and those ECMP combinations where no cardiomyocytes were observed contracting (red dots).

based on structural, electrophysiological, and biomarker characteristics (See Table S1). To effectively identify AP morphology, we must determine the speed of the different phases that make up the action potential duration (APD) as well as the time difference between distinct regions of the ADP – these are often written as ADP followed by a number to signify the time difference between a percentage of the contraction time and the pairing percentage on the relaxation time. This type of analysis is often referred to as the indices of triangulation and can help identify chamber-specific cell types through discrete characteristics. For example, nodal cells often have a slow AP velocity when performing patch clamping [87,88]. We predicted this to be ~ 5–10 μm/s from the data collected of the AP morphologies of the 20 groups of contracting cardiomyocytes. Nodal cells often lack an early repolarization phase and show a plateau in the repolarization phase so as not to induce quick repolarization in surrounding atrial tissue [89]. The characteristics of the repolarization phase of nodal cells show an APD50 and APD90 of 100 and 150 ms, respectively, with the indices APD50/APD90 and APD90-APD50 of approximately 0.6 and 50 ms, respectively [87]. Additionally, the ratio of APD30-40/APD70-80 will show roughly 0.65 [29].

Owing to their imperative role in rapidly transmitting electrical signals, conductive cells exhibit a notably swift upstroke velocity, calculated to exceed 100 μm/s [90]. These cells share a repolarization phase, akin to ventricular myocytes but with a lower amplitude, this feature is attributed to their close proximity in vivo [90,91]. Notably, conductive cells demonstrate extended action potential durations, with APD50 and APD90 measuring approximately ~ 220 ms and ~ 300 ms, respectively [91]. Key indices such as APD50/APD90 and APD90-APD50 are estimated to be around 0.7 and 80 ms, respectively [90]. Our calculations indicate that the ratio of APD30-40/APD70-80 should fall within the range of 0.6–0.8.

Atrial cells typically exhibit an intermediate action potential (AP) velocity, falling between nodal and ventricular cells, with our calculations indicating this to be approximately 20 μm/s [92,93]. In general, atrial cells are characterized by a lack of a plateau phase and a more triangular AP morphology. The variability in AP morphologies of atrial cells introduces a considerable window for triangulation indices. The repolarization phase for atrial cells may exhibit an APD50 and APD90 values around 25 ms and 200 ms, respectively, although other studies report APD50 and APD90 closer to 200 ms and 400 ms, respectively [94–97]. Consequently, repolarization indices such as APD50/APD90 and APD90-APD50 also exhibit a range between 0.2–0.5 and 175–200 ms, respectively [95,97]. Additionally, the ratio of APD30-40/APD70-80 is estimated to have a value of approximately 0.7–0.9 [29].

Ventricular myocytes are characterized by their predominant expression of MLC2v over MLC2a. These cells exhibit a highly organized structure and often display faster action potential (AP) velocities similar to conductive cells, with our calculations indicating a velocity of approximately 70–100 μm/s [91,98]. Ventricular cells are renowned for their distinct plateau phase, a feature reflected in their repolarization indices. Given the greater thickness of ventricular tissue compared to atrial tissue, the AP morphology of ventricular cells can vary based on their location, whether towards the epicardium or the internal chamber. Midmyocardial tissue may report APD50 and APD90 values of 200 ms and 270 ms, respectively, while ventricular cells closer to the epicardium may exhibit APD50 and APD90 values of 300 ms and 400 ms [91,98]. This variability results in a range for repolarization indices such as APD50/APD90 and APD90-APD50, estimated to be 0.65–0.85 and 50–130 ms, respectively [98,99]. Additionally, the ratio of APD30-40/APD70-80 is anticipated to have a value of approximately 0.8–1.0 [29].

We conducted an optical mapping study on the 20 ECMP combinations that induced cardiomyocyte contractions, and the results are displayed in Fig. 9 and Figure S17. Particularly focusing on the three ECMP combinations (C1C3FLV, C3C4FV, and C1C3C4V) identified in the t-SNE graph in Fig. 8B for their enhanced maturation characteristics, we observed that all three of these ECMP combinations exhibit similar or improved contraction profile characteristics compared to the control group. This conclusion is based on several key observations. Beat rate variation in these three ECMP groups tends to be lower than in the control group and are significantly different in the C3C4FV group (*t*-test P=0.0067). These lowered beat rate variations indicate a more established contraction frequency and a reduced likelihood of competing pacemaker regions. While two of the three ECMP groups show a similar contraction velocity and contraction duration to the control group, the C3C4FV group shows a significantly lowered contraction velocity and a significantly increased contraction time. In addition, there is a significant difference between the means of the relaxation times of the control and ECMP groups when performing a one-way ANOVA (P=0.0133). The increased contraction velocity, contraction time, and reduced beat rate variation suggest that cardiomyocytes in these ECMP groups possess a more matured phenotype, possibly due to increased ion channel distribution, and or, improved sarcomere alignment which enhances their ability to control the repolarization phase. The increased relaxation duration also implies a more matured phenotype with increased ion channel density and distribution but could also indicate improved retention of calcium in the sarcoplasmic reticulum and improved calcium handling through ion channels in these ECMP groups. The discovery of the reasons for the improved contraction profile metrics falls outside the scope of this study but is an exciting area for future research.

The characterization of cardiomyocyte AP morphology on the 20 ECMP combinations was conducted using the criteria list we developed in Table S1. By applying this criteria list, we assigned a chamber specification to each of the 20 ECMP combinations, as outlined in Table S2. Subsequently, we generated PCA and t-SNE graphs using the AP morphology data derived from the optical mapping study (see Fig. 10). The PCA graph reveals a random distribution of data points without significant clustering. However, when colour-coded based on their assigned chamber specification, evidence of clustering emerges, with certain areas indicating potential crossover between groups. Notably, the scree plot illustrates an elbow for two principal components, and the proportion of variance exceeds the 80 % threshold on the first principal component (Figure S18). When we generated the t-SNE graph for the AP morphology data we saw a similar separation of data points grouping into the chamber specifications we assigned them. To ensure this data was accurate we replicated the t-SNE graph and adjusted the perplexity value between 0–15 to ensure the grouping of data points was consistent (Figure S19). Collectively, this data underscores how the combined analysis of molecular markers and contraction optical mapping can reveal subtle differences in cardiac lineage specification. We believe this demonstrates that specific ECMP combinations have the potential to influence chamber-specification during cardiac differentiation.

Discussion

In this study, we developed an ECMP array to identify how individual matrix proteins and their combinations can influence the proliferation and pluripotency of hESC. We then built on this platform to identify how specific ECMP combinations can aid cardiac differentiation and influence chamber specific characteristics. Previous studies have demonstrated that hESC can show preferences for certain protein combinations for the maintenance of pluripotency similar to commercial substrates [57,59,100]. These studies highlight that there are specific ECMP combinations that can maintain the pluripotency of stem cells for long period in culture and thus alludes to the possibility that alternative ECMP combinations could direct cell fate. The number of literature sources investigating the benefits of ECMP combinations on maintaining stem cell's pluripotency highlights stem cells can be maintained on various ECMP combinations but also indicates that this could be a cell line-specific behaviour. Here we screened 63 ECMP combinations and identified a preference for laminin, vitronectin, collagen I and collagen IV (C1C4LV) for our H9 hESC which displayed good expression of pluripotency markers and consistent proliferation rate compared to Matrigel™. We also demonstrated that hESC on this ECMP combination could

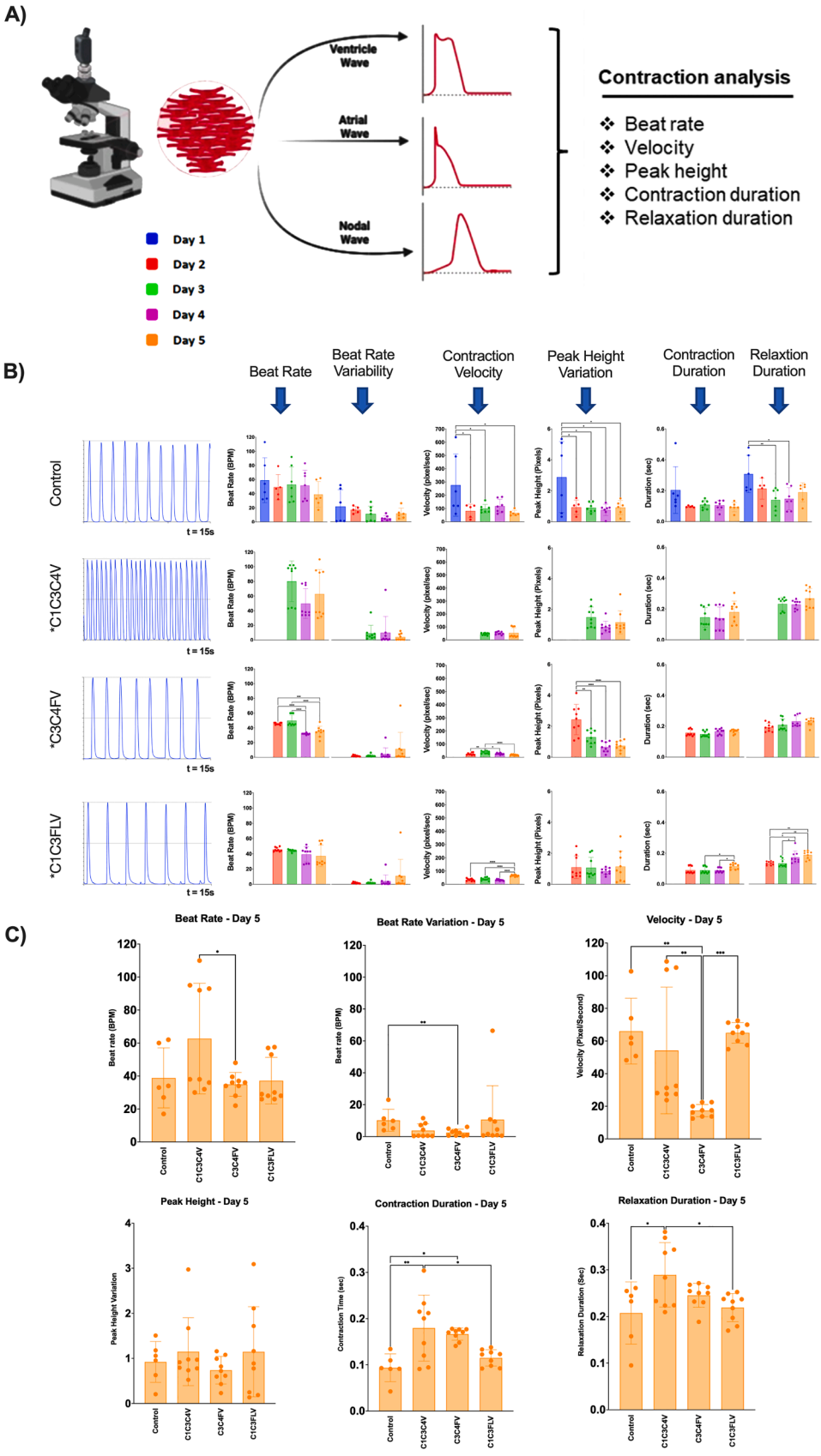

(caption on next page)

Fig. 9. Contraction Profiles for top three ECMP combinations that produced contracting cardiomyocytes and the control group. A) ECMPs featuring contracting cardiomyocytes are optically mapped using a high-speed microscope to compare action potential (AP) morphologies. B) AP morphologies for ECMP combinations for the top three with the control group. The left panel shows the normalized peak height contraction profiles for each ECMP combination as derived from high-speed videos. These profiles are from videos taken on day 5 and are representative average of 9 independent videos taken. The bar charts on the right show the beat rate, beat rate variation, contraction velocity, peak height variation, contraction duration, and relaxation duration of the cardiomyocytes measured over a five-day period. C) Statistical analysis of contraction metrics for select formulations compared to controls. These mean values are averaged from three independent regions within the culture well with videos taken in triplicate with a ten-minute interval between each recording round. * P value < 0.05, ** P value < 0.01, *** P value < 0.001.

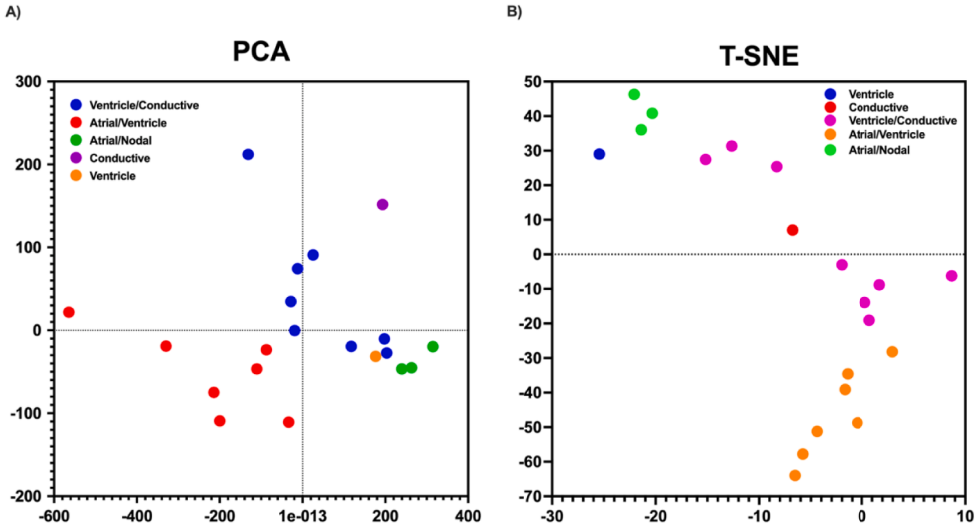

Fig. 10. Principal component analysis (PCA) and T-distributed stochastic neighbor embedding (T-SNE) plot of chamber specifications A) Principal component analysis of all AP morphology measurements for all 20 contracting ECMP combinations. Data points are separated into chamber specific groups, B) t-distributed stochastic neighbor embedding plot of all the 20 AP morphology characteristics. Data points are separated into chamber specific groups.

reach 80 % confluency. while maintaining similar cell morphology and differentiation efficiency when compared to cultures on Matrigel™. When the C1C4LV combination was compared to ECMP combinations with one or more of these ECMP removed, we identified the importance of collagen I and collagen IV, as removal of the collagens negatively affected proliferation and pluripotency. Our study also revealed that whilst certain ECMP combinations could maintain pluripotency, others could increase expression of markers associated with specific germ layers, and hence might influence lineage specification.

The downregulation of pluripotency markers, indicates certain ECMP combinations may induce germ-line differentiation of hESC. Furthermore, specific ECMP combinations can influence precise germ-line differentiation lineages and even enhance cardiac progenitor markers. In many cases, ECMP promoted dual lineage expression of Sox17 and T-brachyury, indicating simultaneous expression of endoderm and mesoderm markers, which we denoted as mes-endodermal populations. This phenomenon was particularly evident in cells cultured on C3C4FLV, which exhibited enhanced co-expression of Sox17 and T-brachyury. However, we also observed instances of single germ-line expression, with mesoderm lineage expression occurring when cells were cultured on single collagen groups (C1, C3, and C4), while endoderm marker expression alone was promoted in more complex combinations (C1C3V, C1C3F, and C3C4). Analysis of cardiac progenitor markers KDR and MESP1 revealed positive correlations between each marker and the mesoderm marker T-brachyury. Therefore, our array-based approach successfully identified ECMP combinations capable of directing pluripotent stem cell populations toward specific germ lineages and the enhanced expression of cardiac progenitor markers. Whilst these results seemed promising ECMPs alone were not able to induce cardiac differentiation to produce contracting cardiomyocytes without the addition of soluble lineage-promoting factors.

Upon subjecting the hESC cultured on the ECMP combinations to a cardiomyocyte differentiation protocol, we observed the derivation of cells exhibiting cardiac progenitor characteristics, characterized by heightened expression of KDR and MESP1. These progenitor cells were more inclined to produce cardiomyocytes with enhanced expression of maturation biomarkers. We conducted a hierarchichal clustering analysis on the index values (refer to Fig. 6) associated with T-brachyury, KDR, and MESP1 both pre and post differentiation. This analysis revealed distinct clusters, with MESP1- (pre and post) combinations prominently positioned at the top and MESP1+ (pre and post) combinations clustered towards the bottom. Immunostaining for maturity markers, including cTnT, MLC2a, and MLC2v, unveiled specific combinations exhibiting elevated MESP1, cTnT, and a high ratio of MLC2v: MLC2a – a characteristic indicative of a mature phenotype in vitro.

Further statistical analysis of cardiac-specific markers across all 63 ECMP combinations pinpointed unique clusters – C1C3FLV, C3C4FV, and C1C3C4V – on the t-distributed stochastic neighbor embedding (t-SNE) plot. These combinations demonstrated optimal characteristics for fostering cardiomyocyte differentiation. Video analysis provided additional insights, revealing that 20 out of the 63 ECMP combinations induced robust contraction post-differentiation, including the three optimal matrices mentioned above. To refine our findings, we developed a custom chamber specific criterion list, incorporating our experimental data and insights from existing literature (refer to Tables S1 and S2). The criteria list in these tables combined expression data, AP morphology data, and morphological information which we used to predict the chamber specification of the contracting cardiomyocytes generated on each of the 20 ECMP combinations. When we performed subsequent PCA and t-SNE analysis on the AP morphology data gathered from the 20 ECMP combinations, we found an accurate alignment between our predictions and the clustering of groups (refer to Fig. 10).

Although the cardiac differentiation pathway is well defined in the literature with a variety of protein biomarkers that can indicate the stage

of differentiation (refer to Fig. 1), we discovered certain combinations of ECMP that favour the expression of cardiomyocytes that do not necessarily align with expected biomarker expression pathways. Biomarker expressions for the early stages of differentiation showed us that many of the ECMP combinations promoted co-expression of germ layer markers, suggesting the potential to guide intermediate progenitor populations (e.g., like SOX17+T-Brachyury+ mes-endodermal cells). Throughout our study, we investigated the expression of ten well-known biomarkers in the cardiomyocyte differentiation lineage. We acknowledge that we did not investigate the specific influences the ECMP had on the heterogeneity of cell types which will be an important undertaking in future translation of our approach. Whilst modern cardiac differentiation protocols have had success in producing cardiomyocytes that could potentially be used in pharmacological testing and cell therapies, it is apparent that the next stage of differentiation protocols will need to utilise refined protein substrates to ensure consistent purity of cardiomyocyte populations with desirable functional characteristics.

Conclusions

In summary, we employed our ECMP microarray to investigate the differentiation potential of hESC on ECMP combinations that differ from commercial substrates. This endeavour lead to the discovery of ECMP combinations that promote various aspects of pluripotency and proliferation and others that help guide cardiomyocyte differentiation. Integrating this array approach with modern cardiac differentiation protocols allowed us to systematically assess cardiomyocyte lineage specification across different ECMP combinations and revealed specific matrices that enhance cardiomyocyte maturation and guide differentiation to chamber-specific cell types. Our findings tell us that future explorations of how the ECMP substrate influences chamber-specific differentiation should investigate the intricate interplay ECMPs have in promoting non-cardiac lineages to better understand the effect this has on the maturation and chamber specification of cardiomyocytes. This exploration holds the promise of significantly improving our understanding of cardiac differentiation methodologies, contributing not only to the enhanced precision of cardiac models in safety pharmacology but also facilitating the development of improved cell therapies in the pursuit of a cure for cardiac disorders. Furthermore, this platform will prove useful for development of cultureware for cell production and manufacturing, with scope for precise matrix formulations serving to complement advanced bioreactor technologies, where dynamic mechanical and electrical stimulation can be employed for further cell and tissue maturation.

Material and methods

Array fabrication

Collagen 1 (Advanced Biomatrix, #5007) and collagen 3 (Advanced Biomatrix, #5021) are received in solution at a concentration of 3 mg/mL and 1 mg/mL, respectively. We immediately dilute both collagen solutions down to 25 μg/mL in 0.01 mol HCL solution in

DPBS prior to coating culture surfaces. Collagen 4 (Advanced Biomatrix, #5016) is received as 5 mg powder. We reconstitute the collagen 4 powder by adding 5 mL of cold 0.25 % acetic acid (Chem Supply Pty Ltd Australia, AA009) and mixing through gentle pipetting. We then incubate the reconstituted powder at 2-8oC with gentle swirling. We then dilute the 1 mg/mL solution down to 25μg/*mL* in 0.25 % acetic acid immediately prior to coating culture surfaces. Fibronectin (ThermoFisher Scientific, #33016015) is received as a 5 mg lyophilized powder. We reconstitute the powder by adding 5 mL of warmed sterile 1X DPBS and allow it to dissolve at 37oC for 30 min. Any undissolved material can be gently separated apart with sterile stainless-steel forceps until fully dissolved. Reconstituted fibronectin is then aliquoted into 25 μL volumes and stored at −20oC. Fibronectin is thawed and diluted to 25μg/*mL* in 1 mL of sterile DPBS immediately prior to coating culture surfaces. Laminin (ThermoFisher Scientific, #23017015) is received as a 1 mg/mL solution in

0.15 M NaCl. To avoid repeated freeze/thaw cycles, the laminin is aliquoted into 25 μL.

volumes and stored at −20oC. Laminin is thawed and diluted to 25μg/*mL* in sterile 1x DPBS prior to coating culture surfaces. Vitronectin (ThermoFisher Scientific, #A14700) is received as a solution at a concentration of 0.5 mg/mL. To avoid repeated freeze/thaw cycles, vitronectin is aliquoted in 50 μL volumes and stored at −80oC. Vitronectin is thawed and the 50 μL volume is diluted to a concentration of 25μg/*mL* in 1 mL of sterile 1x DPBS prior to coating culture surfaces.Proteins were distributed in a 96-well plate – Corning 96 well TC-treated Microplates (Merck Australia, CLS3997) using a manual 200uL micropipette following the schematic in Fig. 2. Matrigel-coated wells were prepared using Corning Matrigel™ hESC-Qualified Matrix, LDEV-free (Corning, 354277, Lot# 1236001). Matrigel was diluted with a dilution factor of 10.84μL/mL in Gibco BenchStable DMEM/F12 (ThermoFisher Scientific Australia, A4192002) and dispensed at 85μL/well. Before seeding, the 96-well plate was placed in a humidified incubator set to 37 °C and 5 % CO2. Plates are either immediately seeded following incubation or are wrapped in parafilm and tin foil and stored at 4 °C for up to 5 days.

Stem Cell Culture

The H9 hESC culture media was mTeSR™ Plus Basal Medium supplemented with mTeSR™ Plus 5x supplement (StemCell Technologies, #100–0276). Cells had media exchanged daily and are passaged weekly in 50μm colonies by gentle dissociation with ReLeSR™ (StemCell Technologies, #05872) for 5 min at 37 °C followed by gentle tapping of the culture dish. Cell clusters are then collected with a wide-mouth 2 mL serological pipette and are agitated by gentle vortexing until most colonies measure ~ 50μ*m* (observed under a microscope). hESC are passaged onto the ECMP array as single cells by exposure to Accutase™ (StemCell Technologies, #07920) for 5 min at 37 °C followed by centrifugation at 300g for 3 min. Cells are re-suspended in culture media supplemented with the RHO/ROCK pathway inhibitor Y-27632 (StemCell technologies, #72304) at a final concentration of 5 μM/mL. hESC are seeded directly into the ECMP array at a seeding density of $1.24x10^4 cells/cm^2$ and incubated in Y27632 supplemented media for 24 h before washing and replenished with culture media.

Staining, imaging, and analysis

Fixing: Culture media is aspirated, and cells are fixed in 4 % PFA for 20 min. **Permeabilize:** Fixed cells are then permeabilized in 0.1 % Triton X-100 diluted in DPBS at room temperature for 30 min. **Blocking:** Cells are blocked by incubation in 1 % BSA at room temperature for 15 min. **Primary antibodies:** primary antibodies used in this study are listed in supplementary Table S3. Cells are stained using antibodies diluted 1:300 in 1 % BSA and incubated for 24 h at 4 °C. Primary antibodies are washed away by one wash in DPBS followed by 2x15minute incubations in DPBS. **Secondary antibodies:** secondary antibodies used in this study are listed in supplementary Table S3. Cells are stained using antibodies diluted 1:300 in 1 % BSA and incubated for 24 h at 4 °C. Secondaries are then washed away by 1x wash in DPBS followed by 2x15minute incubations in DPBS. Unless nuclear material is stained with Hoescht 33,342 (ThermoFisher Scientific Australia, 62249), all cells are then mounted by inversion onto VECTASHEILD antifade mounting medium with DAPI (Fisher Scientific, NC9524612) and sealed with clear nail polish. Confocal imaging was performed on the Zeiss LSM 800 with an inverted Axio Observer Z1 with two multi-alkali (MA) PMT (typical QE 25 %) detectors. The microscope settings were as follows: objective 20x with a 1x crop area, pinhole 460 μm, scan speed 0.52 μs/pixel, 1024x1024pixel image with 2x averaging line-by-line single-

directional mean intensity 8bit format. Images were collected using the following detection mirror settings Hoechst33342 & DAPI (400–496 nm), Alexa Fluor™ 488 & ATTO 488 (490–583 nm), CF™ 555 & Alexa Fluor™ 594 (594–637 nm), Atto 647 N & CF™ 647 (647–700 nm). Fluorophores were excited using the following light sources: 405 nm (3.5 %), 488 nm (4.5 %), 561 nm (4.5 %), and 640 nm (5 %), respectively. To eliminate crosstalk between channels, the images were collected sequentially. The maximum intensity of images was attained by gain alterations to a point just below saturation in the brightest images, with settings maintained across all samples.

Cardiac differentiation

H9 hESC cultured at a seeding density of $1.24x10^4 cells/cm^2$ would reach confluency on day 5 (120 h) when seeded onto the Matrigel-coated wells. H9 hESC on the ECMP combinations had varying confluency levels on day 5 (120 h). When the differentiation protocol starts, we denote this day as day 0 as a reference for the following steps. On day 0, all cells' media was exchanged for the differentiation media RPMI (ThermoFisher Scientific AU, 11875093) supplemented with 2 % B27 Minus insulin (ThermoFisher Scientific AU, A1895601). The cells were treated with GSK3b inhibitor CHIR-98014 (StemCell Technologies AU, 73042) at a concentration of 0.8 μM. At exactly 24 h (day 1) the differentiation media is aspirated and cells were washed with fresh differentiation media. The culture wells are then replenished with differentiation media and cells are left for 48 h (Days 1 – 3). On day 3 50 % of the culture media is aspirated and replaced with fresh differentiation media supplemented with the Wnt-inhibitor Wnt-C59 (Trocis, 5148) at a concentration of 2 μM in the final volume. Cells are then incubated for 48 h (days 3–5). On day five, culture media is aspirated and replenished with fresh differentiation media and cells are left to incubate for 48 h (Day 5–7). On Day 7, cell media is aspirated and replaced with RPMI supplemented with B27 x50 (ThermoFisher Scientific AU, 17504044). Cells receive media exchanges every 2 days after day 7 with the RPMI media supplement B27 x50. Cardiomyocyte contractions tend to initiate around day 10 of the differentiation protocol and can be kept for long periods in incubation. The cells were incubated at 37 °C in a humidified atmosphere with 5 % CO2.

High-speed camera

Cardiomyocyte contractions were captured on a Zeiss Observer Z1 Spinning disk and TIRF microscope. The microscope is fitted with a temperature-controlled microscope enclosure and stage insert with CO_2 flow regulator. It also featured a motorized stage and Hamamatsu ORCA-FLASH 4.0 Digital CMOS Camera. This setup made it possible to perform long-term live-cell imaging experiments. The microscope settings were as follows: objective 4x with a 1x crop area, temperature setting of 37oC and 5 % CO2. Images and video of contracting cardiomyocytes were taken with a frame rate of 100 fps with variable contrast for 15 s to generate 1500 framed.AVI files. A motorized stage was used to create a list of 5 different locations of contracting cardiomyocytes in each culture well; these locations had 3 videos taken with at least 5 min between video captures and were repeated daily for a period of 5 days. Contraction data was gathered using the high-speed video analysis platforms, Pulse Video Analysis software [84] and the MUSCLEMOTION plugin for ImageJ [101]. The Pulse Video Analysis software is a web-based portal that requires uploading the 15 s.AVI files and setting the parameters on the webpage as follows: frame rate set at 100fps, select type of video analysis set to contractility (brightfield), remove noisy signals set to yes. The upload option then allows for the specification of groups meaning all videos for a particular day, culture plate, and experimental parameters can be listed. This grouped upload allows for a streamlined analysis as automatic averaging of all parameters in each group is performed. The data files that are generated are separated for each video. The individual videos are divided into 25 quadrants and for each quadrant, a contraction and velocity trace are plotted and given in both data and graphical form. In addition, an image of the video's visual field is provided with a description of the active quadrants (areas of contractility) grouped based on their similarity in contraction profile. Finally, a summary document is provided that shows the profile metrics for each quadrant. The metrics measured include Beat Rate (bpm), Minimum Beat Rate (bpm), Maximum Beat Rate (bpm), Beat Rate Variation, Velocity (pixels/sec), Contraction Displacement (pixels), Peak Height Variation, Duration 75 % (sec), Duration 50 % (sec), Contraction Time (sec), Relaxation Time (sec), and Prevalence (%). The high-speed videos were also analyzed using the MUSCLEMOTION plugin for ImageJ which was downloaded from the following link (https://www.ahajournals.org/doi/suppl/https://doi.org/10.1161/CIRCRESAHA.117.312067). This software stipulates the parameters for video quality with a minimum frame rate of 75fps, adequate lighting and contrast, and a.AVI or.TIFF file type. The limitations of this software include the computer's hardware in which the analysis is carried out. Suppose the files being analyzed are of significant quality. In that case, the memory of the computer must be at least 32 GB to ensure cashed files don't exceed the physical memory of the computer. The MUSCLEMOTION software required a more experimental approach as many analysis parameters can be adjusted and an understanding of videography dynamics in combination with a good knowledge of cardiomyocyte contraction profiles is needed. The output files from the MUSCLEMOTION software are similar to the Pulse Video Analysis software but do allow for extra percentages of transients which are commonly used in cardiomyocyte contraction profile analysis.

CRediT authorship contribution statement

Jake Ireland: Writing – review & editing, Writing – original draft, Visualization, Methodology, Investigation, Formal analysis, Data curation, Conceptualization. **Kristopher A. Kilian:** Writing – review & editing, Supervision, Resources, Project administration, Methodology, Investigation, Funding acquisition, Conceptualization.

Declaration of competing interest

The authors declare that they have no known competing financial interests or personal relationships that could have appeared to influence the work reported in this paper.

Data availability

Data will be made available on request.

Acknowledgements

J.I. acknowledges scholarship support from the Graduate Research School at the University of New South Wales, Australia (UNSW) with the University International Postgraduate Award (UIPA). This work was supported through funding from the Australian Research Council, Australia Grant FT180100417 (K.A.K.), the National Health and Medical Research Council, Australia Grant APP1185021 (K.A.K.), NSW Health Cardiovascular Research Capacity Program Senior Researcher Grant (K.A.K.), and the National Cancer Institute of the National Institutes of Health, United States Grant R01CA251443 (K.A.K.). The authors acknowledge the help and support of Dr Alex Macmillan and Dr Michael Carnell at the Katharina Gaus Light Imaging Facility (KGLMF) of the UNSW Mark Wainwright Analytical Centre, Australia. In addition, the authors acknowledge the help and support of the staff at CuriBio with the Pulse™ High-throughput video contractility analysis software.

Appendix A. Supplementary data

Supplementary data to this article can be found online at https://doi.

org/10.1016/j.mbplus.2024.100160.

References

[1] D.A. Taylor, S.C. Silvestry, S.P. Bishop, B.H. Annex, R.E. Lilly, D.D. Glower, et al., Delivery of primary autologous skeletal myoblasts into rabbit heart by coronary infusion: a potential approach to myocardial repair, Proceedings of the Association of American Physicians 109 (3) (1997) 245–253.

[2] C.E. Murry, M.H. Soonpaa, H. Reinecke, H. Nakajima, H.O. Nakajima, M. Rubart, et al., Haematopoietic stem cells do not transdifferentiate into cardiac myocytes in myocardial infarcts, Nature 428 (6983) (2004) 664–668.

[3] J.J.H. Chong, C.E. Murry, Cardiac regeneration using pluripotent stem cells—Progression to large animal models, Stem Cell Research 13 (3) (2014) 654–665.

[4] C.E. Murry, G. Keller, Differentiation of Embryonic Stem Cells to Clinically Relevant Populations: Lessons from Embryonic Development, Cell 132 (4) (2008) 661–680.

[5] C. Kane, C.M.N. Terracciano, Concise Review: Criteria for Chamber-Specific Categorization of Human Cardiac Myocytes Derived from Pluripotent Stem Cells, Stem Cells 35 (8) (2017 Aug 1) 1881–1897.

[6] W. Zimmermann, M. Didie, S. Doker, I. Melnychenko, H. Naito, C. Rogge, et al., Heart muscle engineering: An update on cardiac muscle replacement therapy, Cardiovascular Research 71 (3) (2006 Aug 1) 419–429.

[7] T. Rozario, D.W. DeSimone, The extracellular matrix in development and morphogenesis: a dynamic view, Developmental Biology 341 (1) (2010 May 1) 126–140.

[8] B. Joddar, S.L. Natividad-Diaz, A.E. Padilla, A.A. Esparza, S.P. Ramirez, D. R. Chambers, et al., Engineering approaches for cardiac organoid formation and their characterization, Translational Research 250 (2022 Dec) 46–67.

[9] M. Sahara, Recent Advances in Generation of In Vitro Cardiac Organoids, International Journal of Molecular Sciences 24 (7) (2023 Mar 26) 6244.

[10] D.M. Lyra-Leite, Ó. Gutiérrez-Gutiérrez, M. Wang, Y. Zhou, L. Cyganek, P. W. Burridge, A review of protocols for human iPSC culture, cardiac differentiation, subtype-specification, maturation, and direct reprogramming, STAR Protoc. 3 (3) (2022 Sep 16) 101560.

[11] C.L. Mummery, J. Zhang, E.S. Ng, D.A. Elliott, A.G. Elefanty, T.J. Kamp, Differentiation of human embryonic stem cells and induced pluripotent stem cells to cardiomyocytes: a methods overview, Circulation Research 111 (3) (2012 Jul 20) 344–358.

[12] T.C. Sung, C.H. Liu, W.L. Huang, Y.C. Lee, S.S. Kumar, Y. Chang, et al., Efficient differentiation of human ES and iPS cells into cardiomyocytes on biomaterials under xeno-free conditions, Biomaterials Science 7 (12) (2019) 5467–5481.

[13] D. Turner, A.C. Rieger, W. Balkan, J.M. Hare, Clinical-based Cell Therapies for Heart Disease—Current and Future State, Rambam Maimonides Med J. 11 (2) (2020 Apr 29) e0015.

[14] R. Zhu, M.A. Millrod, E.T. Zambidis, L. Tung, Variability of Action Potentials Within and Among Cardiac Cell Clusters Derived from Human Embryonic Stem Cells, Scientific Reports 6 (1) (2016 Jan 5) 18544.

[15] Food and Drug Administration, HHS. International Conference on Harmonisation; guidance on S7B Nonclinical Evaluation of the Potential for Delayed Ventricular Repolarization (QT Interval Prolongation) by Human Pharmaceuticals; availability. Notice. Fed Regist. 2005 Oct 20;70(202):61133–4.

[16] H. Wu, A. Zou, F. Xie, Y. Du, Y. Cao, Y. Liu, et al., Effect of matrine on human ether à go-go related gene (HERG) channels expressed in Chinese hamster ovary cells, Chinese Journal of Integrative Medicine 16 (5) (2010 Oct) 430–434.

[17] B.D. Walker, S.M. Valenzuela, C.B. Singleton, H. Tie, J.A. Bursill, K.R. Wyse, et al., Inhibition of HERG channels stably expressed in a mammalian cell line by the antianginal agent perhexiline maleate, British Journal of Pharmacology 127 (1) (1999 May) 243–251.

[18] Withdrawal of Troglitazone and Cisapride. JAMA. 2000 May 3;283(17):2228.

[19] D. Josefson, Hay fever drug to be banned by the FDA, BMJ 314 (7076) (1997 Jan 25) 247.

[20] W.J. Crumb, J. Vicente, L. Johannesen, D.G. Strauss, An evaluation of 30 clinical drugs against the comprehensive in vitro proarrhythmia assay (CiPA) proposed ion channel panel, Journal of Pharmacological and Toxicological Methods 81 (2016) 251–262.

[21] E. Passini, O.J. Britton, H.R. Lu, J. Rohrbacher, A.N. Hermans, D.J. Gallacher, et al., Human In Silico Drug Trials Demonstrate Higher Accuracy than Animal Models in Predicting Clinical Pro-Arrhythmic Cardiotoxicity, Frontiers in Physiology 8 (2017) 668.

[22] C. Robertson, D.D. Tran, S.C. George, Concise review: maturation phases of human pluripotent stem cell-derived cardiomyocytes, Stem Cells 31 (5) (2013 May) 829–837.

[23] X. Lian, C. Hsiao, G. Wilson, K. Zhu, L.B. Hazeltine, S.M. Azarin, et al., Robust cardiomyocyte differentiation from human pluripotent stem cells via temporal modulation of canonical Wnt signaling, PNAS 109 (27) (2012 Jul 3) E1848–E1857.

[24] J. Zhang, M. Klos, G.F. Wilson, A.M. Herman, X. Lian, K.K. Raval, et al., Extracellular Matrix Promotes Highly Efficient Cardiac Differentiation of Human Pluripotent Stem Cells: The Matrix Sandwich Method, Circulation Research 111 (9) (2012 Oct 12) 1125–1136.

[25] P.W. Burridge, E. Matsa, P. Shukla, Z.C. Lin, J.M. Churko, A.D. Ebert, et al., Chemically defined generation of human cardiomyocytes, Nature Methods 11 (8) (2014 Aug) 855–860.

[26] A. Haase, R. Olmer, K. Schwanke, S. Wunderlich, S. Merkert, C. Hess, et al., Generation of induced pluripotent stem cells from human cord blood, Cell Stem Cell 5 (4) (2009 Oct 2) 434–441.

[27] A. Moretti, M. Bellin, A. Welling, C.B. Jung, J.T. Lam, L. Bott-Flügel, et al., Patient-Specific Induced Pluripotent Stem-Cell Models for Long-QT Syndrome, The New England Journal of Medicine 363 (15) (2010 Oct 7) 1397–1409.

[28] I. Itzhaki, L. Maizels, I. Huber, L. Zwi-Dantsis, O. Caspi, A. Winterstern, et al., Modelling the long QT syndrome with induced pluripotent stem cells, Nature 471 (7337) (2011 Mar 10) 225–229.

[29] J. Ma, L. Guo, S.J. Fiene, B.D. Anson, J.A. Thomson, T.J. Kamp, et al., High purity human-induced pluripotent stem cell-derived cardiomyocytes: electrophysiological properties of action potentials and ionic currents, American Journal of Physiology. Heart and Circulatory Physiology 301 (5) (2011 Nov) H2006–H2017.

[30] H.D. Devalla, V. Schwach, J.W. Ford, J.T. Milnes, S. El-Haou, C. Jackson, et al., Atrial-like cardiomyocytes from human pluripotent stem cells are a robust preclinical model for assessing atrial-selective pharmacology, EMBO Molecular Medicine 7 (4) (2015 Apr) 394–410.

[31] Z. Weng, C.W. Kong, L. Ren, I. Karakikes, L. Geng, J. He, et al., A simple, cost-effective but highly efficient system for deriving ventricular cardiomyocytes from human pluripotent stem cells, Stem Cells and Development 23 (14) (2014 Jul 15) 1704–1716.

[32] S.L.K. Bowers, I. Banerjee, T.A. Baudino, The extracellular matrix: at the center of it all, Journal of Molecular and Cellular Cardiology 48 (3) (2010 Mar) 474–482.

[33] Williams C, Black LD. The Role of Extracellular Matrix in Cardiac Development. In: Suuronen EJ, Ruel M, editors. Biomaterials for Cardiac Regeneration [Internet]. Cham: Springer International Publishing; 2015 [cited 2024 Jan 31]. p. 1–35. Available from: https://link.springer.com/10.1007/978-3-319-10972-5_1.

[34] J.G. Jacot, J.C. Martin, D.L. Hunt, Mechanobiology of cardiomyocyte development, Journal of Biomechanics 43 (1) (2010 Jan) 93–98.

[35] M. Mollova, K. Bersell, S. Walsh, J. Savla, L.T. Das, S.Y. Park, et al., Cardiomyocyte proliferation contributes to heart growth in young humans, PNAS 110 (4) (2013 Jan 22) 1446–1451.

[36] U. Hedin, B.A. Bottger, E. Forsberg, S. Johansson, J. Thyberg, Diverse effects of fibronectin and laminin on phenotypic properties of cultured arterial smooth muscle cells, The Journal of Cell Biology 107 (1) (1988 Jul) 307–319.

[37] Hynes RO. Fibronectins [Internet]. New York, NY: Springer New York; 1990 [cited 2024 Jan 31]. (Rich A, editor. Springer Series in Molecular Biology). Available from: http://link.springer.com/10.1007/978-1-4612-3264-3.

[38] F. Farhadian, F. Contard, A. Corbier, A. Barrieux, L. Rappaport, J.L. Samuel, Fibronectin expression during physiological and pathological cardiac growth, Journal of Molecular and Cellular Cardiology 27 (4) (1995 Apr) 981–990.

[39] L.K. Hornberger, S. Singhroy, T. Cavalle-Garrido, W. Tsang, F. Keeley, M. Rabinovitch, Synthesis of Extracellular Matrix and Adhesion Through β_1 Integrins Are Critical for Fetal Ventricular Myocyte Proliferation, Circulation Research 87 (6) (2000 Sep 15) 508–515.

[40] J.A. Feinstein, D.W. Benson, A.M. Dubin, M.S. Cohen, D.M. Maxey, W.T. Mahle, et al., Hypoplastic Left Heart Syndrome, Journal of the American College of Cardiology 59 (1) (2012 Jan) S1–S.

[41] F. Li, X. Wang, J.M. Capasso, A.M. Gerdes, Rapid transition of cardiac myocytes from hyperplasia to hypertrophy during postnatal development, Journal of Molecular and Cellular Cardiology 28 (8) (1996 Aug) 1737–1746.

[42] L.A. Samsa, B. Yang, J. Liu, Embryonic cardiac chamber maturation: Trabeculation, conduction, and cardiomyocyte proliferation, American J of Med Genetics Pt c. 163 (3) (2013 Aug) 157–168.

[43] N.G. Frangogiannis, The extracellular matrix in myocardial injury, repair, and remodeling, The Journal of Clinical Investigation 127 (5) (2017 May 1) 1600–1612.

[44] R.O. Cannon, J.W. Butany, B.M. McManus, E. Speir, A.B. Kravitz, R. Bolli, et al., Early degradation of collagen after acute myocardial infarction in the rat, The American Journal of Cardiology 52 (3) (1983 Aug) 390–395.

[45] P.E. Shamhart, J.G. Meszaros, Non-fibrillar collagens: key mediators of post-infarction cardiac remodeling? Journal of Molecular and Cellular Cardiology 48 (3) (2010 Mar) 530–537.

[46] G.M. Fomovsky, J.W. Holmes, Evolution of scar structure, mechanics, and ventricular function after myocardial infarction in the rat, The American Journal of Physiology - Heart and Circulatory Physiology 298 (1) (2010 Jan) H221–H228.

[47] G. Gaggi, A. Di Credico, P. Izzicupo, S. Sancilio, M. Di Mauro, G. Iannetti, et al., Decellularized Extracellular Matrices and Cardiac Differentiation: Study on Human Amniotic Fluid-Stem Cells, IJMS. 21 (17) (2020 Aug 31) 6317.

[48] L. Iop, T. Palmosi, E. Dal Sasso, G. Gerosa, Bioengineered tissue solutions for repair, correction and reconstruction in cardiovascular surgery, Journal of Thoracic Disease 10 (Suppl 20) (2018 Jul) S2390–S2411.

[49] S. Parveen, S.P. Singh, M.M. Panicker, P.K. Gupta, Amniotic membrane as novel scaffold for human iPSC-derived cardiomyogenesis, In Vitro Cellular & Developmental Biology. Animal 55 (4) (2019 Apr) 272–284.

[50] G.R. Liguori, T.T.A. Liguori, S.R. de Moraes, V. Sinkunas, V. Terlizzi, J.A. van Dongen, et al., Molecular and Biomechanical Clues From Cardiac Tissue Decellularized Extracellular Matrix Drive Stromal Cell Plasticity, Frontiers in Bioengineering and Biotechnology 8 (2020) 520.

[51] D.A. Brafman, C. Phung, N. Kumar, K. Willert, Regulation of endodermal differentiation of human embryonic stem cells through integrin-ECMP interactions, Cell Death and Differentiation 20 (3) (2013 Mar) 369–381.

[52] R.H. Xu, R.M. Peck, D.S. Li, X. Feng, T. Ludwig, J.A. Thomson, Basic FGF and suppression of BMP signaling sustain undifferentiated proliferation of human ES cells, Nature Methods 2 (3) (2005 Mar) 185–190.

[53] C.S. Hughes, L.M. Postovit, G.A. Lajoie, Matrigel: A complex protein mixture required for optimal growth of cell culture, Proteomics 10 (9) (2010 May) 1886–1890.

[54] J.D. Tompkins, C. Hall, V.C. Chen, A.X. Li, X. Wu, D. Hsu, et al., Epigenetic stability, adaptability, and reversibility in human embryonic stem cells, PNAS 109 (31) (2012 Jul 31) 12544–12549.

[55] K. Noaksson, N. Zoric, X. Zeng, M.S. Rao, J. Hyllner, H. Semb, et al., Monitoring differentiation of human embryonic stem cells using real-time PCR, Stem Cells 23 (10) (2005) 1460–1467.

[56] O. Genbacev, A. Krtolica, T. Zdravkovic, E. Brunette, S. Powell, A. Nath, et al., Serum-free derivation of human embryonic stem cell lines on human placental fibroblast feeders, Fertility and Sterility 83 (5) (2005 May) 1517–1529.

[57] S.R. Braam, L. Zeinstra, S. Litjens, D. Ward-van Oostwaard, S. van den Brink, L. van Laake, et al., Recombinant vitronectin is a functionally defined substrate that supports human embryonic stem cell self-renewal via alphavbeta5 integrin, Stem Cells 26 (9) (2008 Sep) 2257–2265.

[58] G.M. Beattie, A.D. Lopez, N. Bucay, A. Hinton, M.T. Firpo, C.C. King, et al., Activin A maintains pluripotency of human embryonic stem cells in the absence of feeder layers, Stem Cells 23 (4) (2005 Apr) 489–495.

[59] D.A. Brafman, K.D. Shah, T. Fellner, S. Chien, K. Willert, Defining long-term maintenance conditions of human embryonic stem cells with arrayed cellular microenvironment technology, Stem Cells and Development 18 (8) (2009 Oct) 1141–1154.

[60] C.J. Flaim, D. Teng, S. Chien, S.N. Bhatia, Combinatorial Signaling Microenvironments for Studying Stem Cell Fate, Stem Cells and Development 17 (1) (2008 Feb) 29–40.

[61] C.J. Flaim, S. Chien, S.N. Bhatia, An extracellular matrix microarray for probing cellular differentiation, Nature Methods 2 (2) (2005 Feb) 119–125.

[62] S. Sa, L. Wong, K.E. McCloskey, Combinatorial Fibronectin and Laminin Signaling Promote Highly Efficient Cardiac Differentiation of Human Embryonic Stem Cells, BioResearch Open Access. 3 (4) (2014 Aug) 150–161.

[63] T. Samura, S. Miyagawa, T. Kawamura, S. Fukushima, J. Yokoyama, M. Takeda, et al., Laminin-221 Enhances Therapeutic Effects of Human-Induced Pluripotent Stem Cell-Derived 3-Dimensional Engineered Cardiac Tissue Transplantation in a Rat Ischemic Cardiomyopathy Model, JAHA. 9 (16) (2020 Aug 18) e015841.

[64] Herron TJ, Rocha AMD, Campbell KF, Ponce-Balbuena D, Willis BC, Guerrero-Serna G, et al. Extracellular Matrix–Mediated Maturation of Human Pluripotent Stem Cell–Derived Cardiac Monolayer Structure and Electrophysiological Function. Circ: Arrhythmia and Electrophysiology. 2016 Apr;9(4):e003638.

[65] Cabral-Pacheco GA, Garza-Veloz I, Castruita-De La Rosa C, Ramirez-Acuña JM, Perez-Romero BA, Guerrero-Rodriguez JF, et al. The Roles of Matrix Metalloproteinases and Their Inhibitors in Human Diseases. IJMS. 2020 Dec 20; 21(24):9739.

[66] J.J.H. Chong, X. Yang, C.W. Don, E. Minami, Y.W. Liu, J.J. Weyers, et al., Human embryonic-stem-cell-derived cardiomyocytes regenerate non-human primate hearts, Nature 510 (7504) (2014 Jun) 273–277.

[67] L.B. Hazeltine, M.G. Badur, X. Lian, A. Das, W. Han, S.P. Palecek, Temporal impact of substrate mechanics on differentiation of human embryonic stem cells to cardiomyocytes, Acta Biomaterialia 10 (2) (2014 Feb) 604–612.

[68] M. Tallawi, R. Rai, B. AldoR, K.E. Aifantis, Effect of Substrate Mechanics on Cardiomyocyte Maturation and Growth, Tissue Engineering Part b: Reviews. 21 (1) (2015 Feb) 157–165.

[69] H. Cao, Q. Zhou, C. Liu, Y. Zhang, M. Xie, W. Qiao, et al., Substrate stiffness regulates differentiation of induced pluripotent stem cells into heart valve endothelial cells, Acta Biomaterialia 143 (2022 Apr) 115–126.

[70] Z. Ma, J. Wang, P. Loskill, N. Huebsch, S. Koo, F.L. Svedlund, et al., Self-organizing human cardiac microchambers mediated by geometric confinement, Nature Communications 6 (1) (2015 Jul 14) 7413.

[71] M. Bao, J. Xie, W.T.S. Huck, Recent Advances in Engineering the Stem Cell Microniche in 3D, Advancement of Science 5 (8) (2018 Aug) 1800448.

[72] Werley CA, Chien MP, Gaublomme J, Shekhar K, Butty V, Yi BA, et al. Geometry-dependent functional changes in iPSC-derived cardiomyocytes probed by functional imaging and RNA sequencing. Pesce M, editor. PLoS ONE. 2017 Mar 23;12(3):e0172671.

[73] F.B. Myers, J.S. Silver, Y. Zhuge, R.E. Beygui, C.K. Zarins, L.P. Lee, et al., Robust pluripotent stem cell expansion and cardiomyocyte differentiation *via* geometric patterning, Integrative Biology 5 (12) (2013 Dec 18) 1495–1506.

[74] M.N.T. Le, M. Takahi, K. Ohnuma, Auto/paracrine factors and early Wnt inhibition promote cardiomyocyte differentiation from human induced pluripotent stem cells at initial low cell density, Scientific Reports 11 (1) (2021 Nov 2) 21426.

[75] L. Przybyla, J. Voldman, Probing Embryonic Stem Cell Autocrine and Paracrine Signaling Using Microfluidics, Annual Rev Anal Chem. 5 (1) (2012 Jul 19) 293–315.

[76] S.J. Kattman, T.L. Huber, G.M. Keller, Multipotent Flk-1+ Cardiovascular Progenitor Cells Give Rise to the Cardiomyocyte, Endothelial, and Vascular Smooth Muscle Lineages, Developmental Cell 11 (5) (2006 Nov) 723–732.

[77] A. Bondue, G. Lapouge, C. Paulissen, C. Semeraro, M. Iacovino, M. Kyba, et al., Mesp1 Acts as a Master Regulator of Multipotent Cardiovascular Progenitor Specification, Cell Stem Cell 3 (1) (2008 Jul) 69–84.

[78] M. Wheelwright, J. Mikkila, F.B. Bedada, M.A. Mandegar, B.R. Thompson, J. M. Metzger, Advancing physiological maturation in human induced pluripotent stem cell-derived cardiac muscle by gene editing an inducible adult troponin isoform switch, Stem Cells 38 (10) (2020 Oct 1) 1254–1266.

[79] E. Karbassi, A. Fenix, S. Marchiano, N. Muraoka, K. Nakamura, X. Yang, et al., Cardiomyocyte maturation: advances in knowledge and implications for regenerative medicine, Nature Reviews. Cardiology 17 (6) (2020 Jun) 341–359.

[80] I. Piccini, J. Rao, G. Seebohm, B. Greber, Human pluripotent stem cell-derived cardiomyocytes: Genome-wide expression profiling of long-term in vitro maturation in comparison to human heart tissue, Genomics Data. 4 (2015 Jun) 69–72.

[81] S.W. Kubalak, W.C. Miller-Hance, T.X. O'Brien, E. Dyson, K.R. Chien, Chamber specification of atrial myosin light chain-2 expression precedes septation during murine cardiogenesis, The Journal of Biological Chemistry 269 (24) (1994 Jun) 16961–16970.

[82] T.X. O'Brien, K.J. Lee, K.R. Chien, Positional specification of ventricular myosin light chain 2 expression in the primitive murine heart tube, PNAS 90 (11) (1993 Jun) 5157–5161.

[83] P. Wu, G. Deng, X. Sai, H. Guo, H. Huang, P. Zhu, Maturation strategies and limitations of induced pluripotent stem cell-derived cardiomyocytes, Bioscience Reports 41 (6) (2021). BSR20200833.

[84] M. Maddah, J.D. Heidmann, M.A. Mandegar, C.D. Walker, S. Bolouki, B. R. Conklin, et al., A Non-invasive Platform for Functional Characterization of Stem-Cell-Derived Cardiomyocytes with Applications in Cardiotoxicity Testing, Stem Cell Reports 4 (4) (2015 Apr) 621–631.

[85] Sánchez C, Bueno-Orovio A, Wettwer E, Loose S, Simon J, Ravens U, et al. Inter-Subject Variability in Human Atrial Action Potential in Sinus Rhythm versus Chronic Atrial Fibrillation. Panfilov AV, editor. PLoS ONE. 2014 Aug 26;9(8): e105897.

[86] A.S. Barth, S. Merk, E. Arnoldi, L. Zwermann, P. Kloos, M. Gebauer, et al., Functional profiling of human atrial and ventricular gene expression, Pflügers Archiv - European Journal of Physiology 450 (4) (2005 Jul) 201–208.

[87] A.O. Verkerk, R. Wilders, M.M.G.J. Van Borren, R.J.G. Peters, E. Broekhuis, K. Lam, et al., Pacemaker current (If) in the human sinoatrial node, European Heart Journal 28 (20) (2007 Sep 7) 2472–2478.

[88] H. Irisawa, H.F. Brown, W. Giles, Cardiac pacemaking in the sinoatrial node, Physiological Reviews 73 (1) (1993 Jan 1) 197–227.

[89] M.R. Boyett, H. Honjo, M. Yamamoto, M.R. Nikmaram, R. Niwa, I. Kodama, Downward gradient in action potential duration along conduction path in and around the sinoatrial node, American Journal of Physiology-Heart and Circulatory Physiology. 276 (2) (1999 Feb 1) H686–H698.

[90] N. Nagy, T. Szél, N. Jost, A. Tóth, J. Papp, A. Varró, Novel experimental results in human cardiac electrophysiology: measurement of the Purkinje fibre action potential from the undiseased human heart, Canadian Journal of Physiology and Pharmacology 93 (9) (2015 Sep) 803–810.

[91] C. Patel, J.F. Burke, H. Patel, P. Gupta, P.R. Kowey, C. Antzelevitch, et al., Is there a significant transmural gradient in repolarization time in the intact heart?: Cellular Basis of the T Wave: A Century of Controversy, Circ: Arrhythmia and Electrophysiology. 2 (1) (2009 Feb) 80–88.

[92] A.A. Dawodu, F. Monti, K. Iwashiro, M. Schiariti, R. Chiavarelli, P.E. Puddu, The shape of human atrial action potential accounts for different frequency-related changes in vitro, International Journal of Cardiology 54 (3) (1996 Jun) 237–249.

[93] B. Le Grand, S. Hatem, E. Deroubaix, J.P. Couetil, E. Coraboeuf, Calcium current depression in isolated human atrial myocytes after cessation of chronic treatment with calcium antagonists, Circulation Research 69 (2) (1991 Aug) 292–300.

[94] A. Workman, The contribution of ionic currents to changes in refractoriness of human atrial myocytes associated with chronic atrial fibrillation, Cardiovascular Research 52 (2) (2001 Nov) 226–235.

[95] A. Bukowska, Y. Nikonova, C. Wolke, U. Lendeckel, J. Kockskämper, A. Goette, Anti-inflammatory effects of endothelin receptor blockade in left atrial tissue of spontaneously hypertensive rats, IJC Heart & Vasculature 42 (2022 Oct) 101088.

[96] D. Dobrev, E. Graf, E. Wettwer, H.M. Himmel, O. Hála, C. Doerfel, et al., Molecular Basis of Downregulation of G-Protein–Coupled Inward Rectifying K^+ Current ($I_{K,ACh}$) in Chronic Human Atrial Fibrillation: Decrease in GIRK4 mRNA Correlates With Reduced $I_{K,ACh}$ and Muscarinic Receptor-Mediated Shortening of Action Potentials, Circulation 104 (21) (2001 Nov 20) 2551–2557.

[97] D.R. Van Wagoner, A.L. Pond, M. Lamorgese, S.S. Rossie, P.M. McCarthy, J. M. Nerbonne, Atrial L-Type Ca^{2+} Currents and Human Atrial Fibrillation, Circulation Research 85 (5) (1999 Sep 3) 428–436.

[98] E. Drouin, G. Lande, F. Charpentier, Amiodarone reduces transmural heterogeneity of repolarization in the human heart, Journal of the American College of Cardiology 32 (4) (1998 Oct) 1063–1067.

[99] G.R. Li, J. Feng, L. Yue, M. Carrier, Transmural heterogeneity of action potentials and I_{to1} in myocytes isolated from the human right ventricle, American Journal of Physiology-Heart and Circulatory Physiology. 275 (2) (1998 Aug 1) H369–H377.

[100] T.J. Rowland, L.M. Miller, A.J. Blaschke, E.L. Doss, A.J. Bonham, S.T. Hikita, et al., Roles of Integrins in Human Induced Pluripotent Stem Cell Growth on Matrigel and Vitronectin, Stem Cells and Development 19 (8) (2010 Aug) 1231–1240.

[101] Sala L, Van Meer BJ, Tertoolen LGJ, Bakkers J, Bellin M, Davis RP, et al. MUSCLEMOTION: A Versatile Open Software Tool to Quantify Cardiomyocyte and Cardiac Muscle Contraction In Vitro and In Vivo. Circulation Research [Internet]. 2018 Feb 2 [cited 2024 Feb 6];122(3). Available from: https://www.ahajournals.org/doi/10.1161/CIRCRESAHA.117.312067.

[102] C. De Sousa, S.M. Lopes, R.J. Hassink, A. Feijen, M.A. Van Rooijen, P. A. Doevendans, L. Tertoolen, et al., Patterning the heart, a template for human cardiomyocyte development, Developmental Dynamics 235 (7) (2006 Jul) 1994–2002.

[103] K. Takahashi, S. Yamanaka, Induction of Pluripotent Stem Cells from Mouse Embryonic and Adult Fibroblast Cultures by Defined Factors, Cell 126 (4) (2006 Aug) 663–676.
[104] B. Lo, L. Parham, Ethical Issues in Stem Cell Research, Endocrine Reviews 30 (3) (2009 May 1) 204–213.
[105] P. Menasché, V. Vanneaux, A. Hagège, A. Bel, B. Cholley, A. Parouchev, et al., Transplantation of Human Embryonic Stem Cell-Derived Cardiovascular Progenitors for Severe Ischemic Left Ventricular Dysfunction, Journal of the American College of Cardiology 71 (4) (2018 Jan) 429–438.
[106] Glauche I, Herberg M, Roeder I. Nanog Variability and Pluripotency Regulation of Embryonic Stem Cells - Insights from a Mathematical Model Analysis. Di Bernardo D, editor. PLoS ONE. 2010 Jun 21;5(6):e11238.
[107] E. Karbassi, C.E. Murry, Flexing Their Muscles: Maturation of Stem Cell-Derived Cardiomyocytes on Elastomeric Substrates to Enhance Cardiac Repair, Circulation 145 (18) (2022 May 3) 1427–1430.